

**METHANE HYDRATE FORMATION AND DISSOCIATION:
ROLES OF PROMOTERS**

Kimhak Neak

A Thesis Submitted in Partial Fulfilment of the Requirements
for the Degree of Master of Science
The Petroleum and Petrochemical College, Chulalongkorn University
in Academic Partnership with
The University of Michigan, The University of Oklahoma,
Case Western Reserve University, and Institut Français du Pétrole

บทคัดย่อและแฟ้มข้อมูลฉบับเต็มของวิทยานิพนธ์ตั้งแต่ปีการศึกษา 2011-2554 ที่ให้บริการในคลังปัญญาจุฬาฯ (CUIR)
เป็นแฟ้มข้อมูลของนิสิตเจ้าของวิทยานิพนธ์ที่ส่งผ่านทางบัณฑิตวิทยาลัย

The abstract and full text of theses from the academic year 2011 in Chulalongkorn University Intellectual Repository (CUIR)
are the thesis authors' files submitted through the Graduate School.

Thesis Title: Methane Hydrate Formation and Dissociation: Roles of Promoters

By: Kimhak Neak

Program: Petroleum Technology

Thesis Advisors: Prof. Pramoch Rangsunvigit

Prof. Santi Kulprathipanja

Accepted by The Petroleum and Petrochemical College, Chulalongkorn University, in partial fulfillment of the requirements for the Degree of Master of Science.

..... College Dean
(Prof. Suwabun Chirachanchai)

Thesis Committee:

.....
(Prof. Pramoch Rangsunvigit)

.....
(Dr. Santi Kulprathipanja)

.....
(Assoc. Prof. Siriporn Jongpatiwut)

.....
(Dr. Tanate Danuthai)

ABSTRACT

6073007063: Petroleum Technology Program

Kimhak Neak: Methane Hydrate Formation and Dissociation: Roles of Promoters.

Thesis Advisors: Prof. Pramoch Rangsunvigit Prof. Santi Kulprathipanja 67 pp.

Keywords: Hydrate/ Solidified natural gas/ Induction time/ Nucleation/ Hydrate growth/ Gas uptake/ Amino acid/ Surfactant/ Micelle.

Roles of promoters become necessary in methane hydrate formation for the attempt of gas storage application, but some additives might cause unwanted results in gas recovery. The effects of amino acids (l-leucine and l-valine) and surfactants, sodium dodecyl sulfate (SDS), and methyl ester sulfonate (MES) was investigated at 8 MPa and 2 to 4 °C. L-leucine system enhanced hydrate formation because of its surface activity and surface adsorption at interfaces. A noticeable methane uptake yield was also observed in the l-valine solution. Its influences might be from the nature of l-valine that has non-polar, aliphatic hydrophobic side chain resulting in lower surface activity or surface adsorption at gas/liquid interfaces. Moreover, synergism between MES and SDS was observed with fast kinetics and high gas uptake because of micelle formation to lower the interfacial tension in the solution. At the same scale of the concentration, 0.23 wt% (CMC-SDS), amino acids cannot achieve methane hydrate formation compared to surfactants. The comparison of promoting an effect of each promoter at the optimum concentrations was exhibited by using 0.5 wt% l-leucine, 0.7 wt% l-valine, 0.23 wt% and 0.12 wt%. Although every promoter was possible to achieve high methane uptake, its pros and cons were clearly indicated. The formation with the amino acids was found with much slower formation rate. However, dissociated gas from the surfactants caused a lot of foam that could against the gas release, taking for a longer time to complete the gas recovery, and losing the amount of surfactant. Unlike the surfactants, methane could be recovered from the hydrate formed with the amino acids at a faster rate and reusability.

บทคัดย่อ

นาย คิมแฮค แนค : การเกิดและการสลายตัวของแก๊สมีเทนไฮเดรต: อิทธิพลของตัวเร่ง (Methane Hydrate Formation and Dissociation: Roles of Promoters) อ. ที่ปรึกษา : ศ.ดร. ปราโมช รั้งสรรคร์วิจิตร ดร.สันติ กุลประทีปปัญญา 67 หน้า

สารเติมแต่งมีส่วนช่วยสำคัญทำให้เกิดมีเทนไฮเดรตเพื่อการกักเก็บก๊าซ แต่สารเติมแต่งบางอย่างอาจทำให้เกิดผลลัพธ์ที่ไม่พึงประสงค์ในการกักเก็บก๊าซ ดังนั้นงานนี้จึงศึกษาผลของการใช้สารเติมแต่ง ประเภทกรดอะมิโน ได้แก่ L-Leucine และ L-Valine และประเภทสารลดแรงตึงผิว ได้แก่ โซเดียมโดเดซิลซัลเฟต (SDS) และเมทิลเอสเทอร์ซัลโฟเนต (MES) ที่ ความดัน 8 เมกะปาสคาล อุณหภูมิ 2 ถึง 4 องศาเซลเซียส เพื่อช่วยในการกักเก็บก๊าซ ผลการศึกษาพบว่า L-Leucine ช่วยเพิ่มการเกิดมีเทนไฮเดรต เพราะคุณสมบัติของพื้นที่ผิวช่วยในการดูดซับระหว่างผิวหน้าของก๊าซและของเหลว L-Valine มีส่วนช่วยในการดูดซับก๊าซมีเทนได้ เนื่องจากธรรมชาติของ L-Valine ที่มีคุณสมบัติไม่มีขั้วและไม่ชอบน้ำ อาจทำให้เกิดแรงดูดซับก๊าซต่ำกว่าระหว่างพื้นที่ผิวของก๊าซและของเหลว นอกจากนี้ยังพบว่าการทำงานร่วมกันระหว่าง MES และ SDS ทำให้จลนพลศาสตร์ในการเกิดมีเทนไฮเดรตเร็วขึ้นและการดูดซับก๊าซสูง เนื่องจากการก่อตัวของไมเซลล์เพื่อลดความตึงผิวระหว่างเฟสจากการแทรกซึมในสารละลาย ที่ความเข้มข้นเดียวกัน คือ 0.23 wt% (CMC-SDS) พบว่ากรดอะมิโนไม่ก่อให้เกิดมีเทนไฮเดรตเมื่อเทียบกับการใช้สารลดแรงตึงผิว การเปรียบเทียบผลกระทบของสารเติมแต่ง แต่ละชนิดที่ความเข้มข้นต่างๆ พบว่าความเข้มข้นที่เหมาะสมแสดงคือ 0.5 wt% L-Leucine 0.7 wt% L-Valine 0.23 wt% SDS และ 0.12 wt% MES แม้ว่าสารเติมแต่งทุกชนิดมีความสามารถในการช่วยทำให้เกิดมีเทนไฮเดรตสูง แต่การใช้กรดอะมิโนมีอัตราการเกิดช้ามาก อย่างไรก็ตามการละลายก๊าซจากการใช้สารลดแรงตึงผิวเป็นสารเติมแต่ง ทำให้เกิดโฟมจำนวนมาก การปล่อยก๊าซใช้เวลานาน และยังสูญเสียปริมาณของสารลดแรงตึงผิวอีกด้วย ต่างจากการใช้กรดอะมิโนในการเกิดมีเทนไฮเดรต กรดอะมิโนทำให้เปิดปฏิกิริยาได้เร็วขึ้น สามารถนำกรดอะมิโนกลับมาใช้ใหม่ได้อีกด้วย

ACKNOWLEDGEMENTS

The author is grateful for the full scholarship and full funding of the thesis work provided by the Petroleum and Petrochemical College.

Gratefully acknowledge ASEAN Scholarship of Chulalongkorn University which offers college fee and a monthly allowance for two years.

Gratefully acknowledge Ministry of Mines and Energy (MME), Cambodia, which offers a long-term nomination and budget to pursue a master degree in the college.

Gratefully acknowledge The Center of Excellence on Petrochemical and Materials Technology.

Gratefully acknowledge UOP, A Honeywell Company, Des Plaines, Illinois, USA.

Gratefully thank advisor (Prof. Pramoch Rangsunvigit), co-advisor (Dr. Santi Kulprathipanja), family, Cambodian friends, PPC classmates who always assist and encourage to make this study successful.

TABLE OF CONTENTS

	PAGE
Title page	i
Abstract	iii
Acknowledgements	v
Table of contents	vi
List of tables	ix
List of figures	xi
Abbreviations	xvi
CHAPTER	
I INTRODUCTION	1
II LITERATURE REVIEW	3
2.1 Natural Gas	3
2.2 Natural Gas Hydrates	4
2.3 Gas Hydrate Structures	6
2.3.1 Structure I (sI)	9
2.3.2 Structure II (sII)	10
2.3.3 Structure H (sH)	10
2.4 Gas Hydrate Formation Processes	11
2.4.1 Hydrate Nucleation	14
2.4.2 Hydrate Nucleation Growth	15
2.4.3 Hydrate Equilibrium	19
2.5 Gas Hydrate Dissociation	21
2.6 Hydrate Promoters	23
2.6.1 Kinetic Promoters	23

CHAPTER	PAGE
2.6.2 Thermodynamic Promoters	27
III EXPERIMENTAL	28
3.1 Materials and Equipment	28
3.1.1 Materials	28
3.1.2 Equipment	28
3.1.3 Chemicals	28
3.2 Methodology	29
3.2.1 Experimental Schematic	29
3.2.2 Hydrate Formation Procedure	30
3.2.3 Hydrate Dissociation Procedure	31
IV RESULTS AND DISCUSSION	32
4.1 Effects of L-leucine	32
4.1.1 Methane Hydrate Formation	32
4.1.2 Methane Hydrate Dissociation	36
4.2 Effects of L-valine	39
4.2.1 Methane Hydrate Formation	39
4.2.2 Methane Hydrate Dissociation	43
4.3 Effects of Sodium Dodecyl Sulfate (SDS)	44
4.3.1 Methane Hydrate Formation	44
4.3.2 Methane Hydrate Dissociation	47
4.4 Effects of Methyl Ester Sulfonate (MES)	48
4.4.1 Methane Hydrate Formation	48
4.4.2 Methane Hydrate Dissociation	51
4.5 Comparison	52

CHAPTER	PAGE
4.5.1 Hydrate Formation at a Concentration of 0.23 wt%	52
4.5.2 Hydrate Formation at CMC and Optimum Concentration of Amino Acids	54
4.5.3 Methane Hydrate Dissociation at CMC- surfactants and Optimum Concentration of Amino Acids at 2 °C and 4 °C	58
V CONCLUSION AND RECOMMENDATIONS	61
5.1 Conclusions	61
5.2 Recommendations	62
REFERENCES	63
CURRICULUM VITAE	67

LIST OF TABLES

TABLE	PAGE
2.1	Chemical properties of natural gas (Demirbas, 2010) 3
2.2	Properties of three common unit crystals (Sloan, 2003) 8
4.1	Methane hydrate formation experimental conditions with the presence of l-leucine at 8 MPa and 2 °C 33
4.2	Methane hydrate dissociation at 30 °C from the hydrates formed with different l-leucine concentrations from the formation temperature 2 °C 38
4.3	Methane hydrate formation experimental conditions with the presence of l-valine at 8 MPa and 2 °C 40
4.4	Methane hydrate dissociation at 30 °C from the hydrates formed with different l-valine concentrations from the formation temperature 2 °C 43
4.5	Methane hydrate formation experimental conditions with the presence of SDS at 8 MPa and 2 °C 46
4.6	Methane hydrate dissociation conditions with different SDS concentrations at temperature 30 °C 48
4.7	Methane hydrate formation experimental conditions with the presence of MES at 2 °C and 8 MPa 50
4.8	Methane hydrate dissociation conditions with different MES concentration at 30 °C 52
4.9	Surface tension versus concentrations of l-leucine, l-valine, SDS and MES (Liu et al., 2015; Kile and Chiou, 1989; Chaturvedi et al., 2018) 53
4.10	Methane hydrate formation with the presence of CMC-surfactants and optimum concentration of amino acids at 2 °C 55

TABLE	PAGE
4.11 Methane hydrate formation with the presence of CMC-surfactants and optimum concentration of amino acids at 4 °C	56
4.12 Methane hydrate dissociation conditions with different promoters at temperature 30 °C from formation temperature at 2 °C	58
4.13 Methane hydrate dissociation conditions with different promoters at temperature 30 °C from formation temperature at 2 °C at 4 °C	59

LIST OF FIGURES

FIGURE		PAGE
2.1	Methane gas hydrate sample (Demirbas, 2010).	4
2.2	Distribution of discovered gas hydrate deposits. BSR ^{1/4} deposit located by seismic refraction (Makogon, 2010).	6
2.3	Water-ice-like cage structure (Demirbas, 2010).	7
2.4	Three common hydrate structure compositions (sI, sII, sH) with water cage types that create hydrate structures (Sloan, 2003).	8
2.5	Different five cages that form each three structures: (a) pentagonal dodecahedron (5^{12}), (b) irregular dodecahedron ($4^35^66^3$), (c) tetrakaidecahedron ($5^{12}6^2$), (d) tetrakaidecahedron ($5^{12}6^4$), and (e) icosahedron ($5^{12}6^8$) (Sloan and Koh, 2007).	9
2.6	Gas hydrate of structure I composes of two pentagonal dodecahedrons (5^{12}), and six tetrakaidecahedrons ($5^{12}6^2$), figure a) and b), respectively (Demirbas, 2010).	9
2.7	Gas hydrate of structure II, a) hexakaidecahedron and b) dodecahedron (Demirbas, 2010).	10
2.8	Gas hydrate of structure H, a) pentagonal dodecahedron, b) icosahedron, and c) irregular dodecahedron (Demirbas, 2010).	11
2.9	Curve of gas consumption and time for hydrate formation (Sloan and Koh, 2007).	12
2.10	Hydrate formation schematic represented by gas uptake in an experiment vs time showing three main phases in hydrate formation process: dissolution phase, supersaturated phase, and growth phase (Khurana <i>et al.</i> , 2017).	13
2.11	Temperature and pressure race for formation of simple methane hydrates (Sloan and Koh, 2007).	13

FIGURE	PAGE
2.12 Schematic model of labile cluster growth: a) the initial condition, b) labile cluster, c) agglomeration, and d) primary nucleation and growth (Sloan and Koh, 2007).	16
2.13 Hydrate labile cluster growth mechanism imposed on a pressure-temperature trace (Sloan and Koh, 2007).	16
2.14 Photograph of single hydrate crystals of (a) tetrahydrofuran (sII); (b) tetrahydrofuran (sI) (Sloan and Koh, 2007).	18
2.15 a) Methane hydrate covering the surface of water droplets (1, 2, 3) under high driving force, 10 min after nucleation. Image (4) is a magnified view of droplet (3), and (b) methane hydrate covering two water droplets under low driving force at three different times: (1) at $t = 0$, (2) at $t = 10$ h where the water droplet is covered by hydrate, (3) at $t = 25$ h where the water droplet is covered by hydrate and depressions in the hydrate layer appear (Servio and Englezos, 2003).	19
2.16 Diagram of stability with assuming methane-pure water and methane seawater (Clennell <i>et al.</i> , 1999).	20
2.17 Phase equilibrium diagram for methane hydrate diagram for methane hydrates (Demirbas, 2010).	20
2.18 Schematic of proposed gas hydrate production methods: (a) thermal injection; (b) depressurization; (c) inhibitor injection (Collett, 2002).	22
2.19 Diagram of the phase boundary of methane hydrate formation as a function of temperature pressure with water depth (Koh, 2002).	23
2.20 Surfactant increases formation rate, the quiescent system (Zhong and Rogers, 2000).	24
2.21 Methane hydrate formation rate with and without additives (Fakharian <i>et al.</i> , 2012).	25

FIGURE	PAGE
2.22 Methane uptake kinetics for bulk water and l-leucine aqueous solutions at 273 K (Liu <i>et al.</i> , 2015).	26
2.23 Experimental and predicted hydrate dissociation pressures for the binary and ternary systems of : (O) water + methane, (●) water + methane + acetone, (▼) water + methane + 1,4-dioxane, (□) water + methane + propylene, (■) water + methane + THF, (-) predicted (Seo <i>et al.</i> , 2001).	27
3.1 Schematic diagram of gas hydrate apparatus; a) schematic diagram, b) cross-section of a crystallizer (Siangsai <i>et al.</i> , 2015).	29
4.1 Methane uptake and temperature profiles during hydrate formation in the presence of 0.23 wt% at 8 MPa and 2 °C (Experiment 1, Table 2.1).	34
4.2 Methane uptake and temperature profiles during hydrate formation in the presence of 0.5 wt% at 8 MPa and 2 °C (Experiment 4, Table 4.1).	35
4.3 Methane uptake and temperature profiles during hydrate formation in the presence of 0.7 wt% at 8 MPa and 2 °C (Experiment 7, Table 4.1).	36
4.4 Hydrate formation kinetic plots using different l-leucine concentrations (0.7 wt%, 0.5 wt%, and 0.23 wt% and 0.12 wt%) in an unstirred reactor at 8 MPa and 2 °C (Experimental # 2, 5, and 7, Table 4.1).	37
4.5 Methane released and temperature profiles for the decomposition of hydrates formed with 0.5 wt% l-leucine with temperature driving force of 28 °C (Experiment 12, Table 4.2).	37

FIGURE	PAGE
4.6 Methane released and temperature profiles for the decomposition of hydrates formed with 0.7 wt% l-leucine at temperature driving force of 28 °C (Experiment 15, Table 4.2).	39
4.7 Methane consumption and temperature profiles during hydrate formation in the presence of 0.5 wt% l-valine at 8 MPa and 2 °C (Experiment 21, Table 4.3).	41
4.8 Methane consumption and temperature profiles during hydrate formation in the presence of 0.7 wt% l-valine at 8 MPa and 2 °C (Experiment 25, Table 4.3).	41
4.9 Methane uptake and temperature profiles during hydrate formation in the presence of 0.9 wt% l-valine at 8 MPa and 2 °C (Experiment 27, Table 4.3).	42
4.10 Hydrate dissociation kinetic plots using different l-valine concentrations (0.9 wt%, 0.7 wt%, and 0.5) in an unstirred reactor at 30 °C (Experimental # 29, 32 and 34, Table 4.4).	44
4.11 Hydrate formation kinetic plots using different SDS concentrations (0.23 wt%, 0.12 wt%, and 0.06 wt%), in an unstirred reactor at 2 °C and 8 MPa (Experimental # 38, 41 and 42 Table 4.5).	47
4.12 Hydrate dissociation kinetic plots using different SDS concentrations(0.23 wt%, 0.12 wt%, and 0.06 wt%) in an unstirred reactor at dissociation temperature 30 °C (Experimental # 44, 47 and 48, Table 4.6).	49
4.13 Hydrate formation kinetic plots using different MES concentrations (0.5 wt%, 0.23 wt%, 0.12 wt%, 0.06 wt%, and 0.03 wt%), in an unstirred reactor at 2 °C and 8 MPa (Experimental # 51, 52, 56, 59 and 62, Table 4.7).	51

FIGURE	PAGE
4.14 Hydrate dissociation kinetic plots using different SDS concentrations (0.03 wt%, 0.06 wt%, 0.12 wt%, 0.23 wt% and 0.5 wt%) in an unstirred reactor at dissociation temperature 30 °C (Experimental # 64, 66, 69, 72 and 75, Table 4.8).	53
4.15 Hydrate formation kinetic plots using concentration 0.23 wt% (CMC-SDS) of different promoter (l-leucine, l-valine, SDS and SDS) in an unstirred reactor at 2 °C and 8 MPa (Experimental # 7, 55, 41 and 27).	54
4.16 Hydrate formation of SDS, MES, l-valine, and l-leucine at CMC-SDS (0.23wt%), CMC-MES (0.12wt%), l-valine (0.7wt%), and l-leucine (0.5wt%) respectively, at 2 °C (Experimental # 76, 78, 80, and 83, Table 4.10).	56
4.17 Hydrate formation of SDS, MES, l-valine, and l-leucine at CMC-SDS (0.23wt%), CMC-MES (0.12wt%), l-valine (0.7wt%), and l-leucine (0.5wt%) respectively, at 4 °C (Experimental # 85, 86, 88 and 90, Table 4.11).	57
4.18 Hydrate dissociation of SDS, MES, l-valine, and l-leucine at CMC-SDS (0.23wt%), CMC-MES (0.12wt%), l-valine (0.7wt%), and l-leucine (0.5wt%) respectively, at 30 °C (Experimental # 91, 93, 95 and 98, Table 4.12).	59
4.19 Hydrate dissociation of SDS, MES, L-valine, and l-leucine at CMC-SDS (0.23wt%), CMC-MES (0.12wt%), l-valine (0.7wt%), and l-leucine (0.5wt%) respectively, at 30 °C (Experiment # 100, 101 and 103 Table 4.13).	60

ABBREVIATIONS

ANG	:	adsorbed natural gas
CMC	:	critical micelle concentration
CNG	:	compressed natural gas
CR	:	crystallizer
DOE	:	department of Energy
GHD	:	gas hydrate deposit
MES	:	methyl ester sulfonate
PC	:	personal computer
PT	:	pressure transducer
R	:	reservoir
SDS	:	sodium dodecyle sulfate
SNG	:	solidified natural gas
T1	:	thermocouple number 1
T2	:	thermocouple number 2
T3	:	thermocouple number 3
T4	:	thermocouple number 4
THF	:	tetrahydrofuran

CHAPTER I INTRODUCTION

Natural gas is particularly regarded as the cleanest burning fossil fuel for generating power, heat, cool, and ignition of vehicles. While nature and environmentally-friendly resources have gained attention, natural gas is on the top of the list with low pollution and much less carbon dioxide emission compared to other fuels. Natural gas composes mainly methane (CH_4) about 85% to 95% volume followed by less portion of heavier hydrocarbons like ethane (C_2H_6), propane (C_3H_8), n-butane and isobutane (C_4H_{10}), and pentanes (C_5H_{12}) (Demirbas, 2010).

In commercial term, natural gas handling executes a risk and less efficiency to reach end users. Liquefied natural gas (LNG) is a well-known liquid form of natural gas transportation, which is possible to reduce the volume of about 600 times at very low temperature (112 K) and atmospheric pressure, but it causes boil-off gas and the high cost of liquefaction. Another common approach is compressed natural gas (CNG) with much smaller volume and safety concerns (Veluswamy *et al.*, 2018). Adsorbed natural gas (ANG) is believed as a safer and less expensive approach, which is targeted by US Department of Energy (DOE) for onboard vehicles with 263 v/v at STP and 0.5 g/g of adsorbent gravimetric storage capacity requirement, but it is actively developed to be applicable for small-scale automobiles (Casco *et al.*, 2015).

In the mean time, solidified natural gas (SNG) is very attractive for the optimized natural gas storage and transport in large scale and long distance. SNG is reported as a very stable, safe, and environment-friendly technique by just using water and a very low amount of promoter to increase clathrate hydrate kinetic formation. In natural gas hydrates, natural gas is trapped in molecular form at moderate temperature and pressure, which is almost completely recovered by simple depressurization or minimal thermal stimulation and also a compact mode with high energy content, whereas other technologies are still facing many problems (Veluswamy *et al.*, 2018).

Methane hydrates are a solid ice-like structure of water, which composes guest gas molecules in its cavities. According to Englezos and Lee (2005), 1 m³ of solid methane hydrates releases approximately 170 m³ methane gas at STP, equivalent to 0.55 m³ of methane gas at 35 MPa. From the commercial views, methane hydrates

are preferred to conduct close to ambient temperature and atmospheric pressure. To achieve the commercial target of hydrate production, attempts have been made to produce SNG with the very fast kinetics of hydrate formation, then passed through the dewatering step to hydrate pelletizing units before its storage. However, the challenging problems are in the stage of hydrate formation, which is energy intensive, and also slow kinetics (Veluswamy *et al.*, 2018).

Many early reports have informed that tetrahydrofuran (THF) is the best thermodynamic promoter (Seo *et al.*, 2001). A series of surfactant like sodium dodecyl sulfate (SDS) is the best kinetic promoter at a specific concentration (Kalogerakis *et al.*, 1993), and also reactor designs reported to promote kinetics of methane hydrate within porous materials (Vysniauskas and Bishnoi, 1983). However, surfactants were reported to increase kinetic hydrate formation rate, but they caused foam in the dissociation stage, also disability to do pelletized hydrates with porous materials. According to Liu *et al.* (2015), a series of amino acids were studied and reported to have more advantages as kinetic promoters, biological production, and regeneration. The best performance among l-methionine, l-tryptophan, phenylalanine, l-arginine, l-glutamic acid, and l-histidine is l-leucine, which reaches the gas uptake of 144 mg/g at the same concentration of 5 mol%, (273 K, 9.5 MPa).

The purpose of this work was to compare the effects of various methane kinetic promoters at a specific concentration with an amino acids and surfactants in an unstirred system. In this experiment, effects of l-leucine, l-valine, sodium dodecyl sulfate (SDS), and methyl ester sulfonate (MES) on methane hydrate formation were observed at the same formation and dissociation condition.

CHAPTER II LITERATURE REVIEW

2.1 Natural Gas

Natural gas is considered as a special burning fossil fuel, which is the cleanest one compared to other existing non-renewable energy sources, like coal, and petroleum. In general, it is a naturally occurring hydrocarbon mixture under surfaces, where a huge amount of organic matter buried for many million years of geological time scale and was transformed mainly to series of alkanes by geothermal and underneath pressure. Since the natural gas deposits were discovered, it has been produced from both oil and gas fields; however, the chemical compositions are differences even from the domestic production wells. Commonly natural gas composes of mainly methane, and some other portions are ethane, propane, isobutene, hexane, nitrogen, carbon dioxide, hydrogen, mercaptan, and less other impurities (Demirbas, 2010; Veluswamy, 2015).

Table 2.1 Chemical properties of natural gas (Demirbas, 2010)

Component	Typical analysis (vol%)	Range (vol%)
Methane	94.9	87.0–96.0
Ethane	2.5	1.8–5.1
Propane	0.2	0.1–1.5
Isobutane	0.03	0.01–0.3
n-Butane	0.03	0.01–0.3
Isopentane	0.01	Trace to 0.14
n-Pentane	0.01	Trace to 0.14
Hexane	0.01	Trace to 0.06
Nitrogen	1.6	1.3–5.6
Carbon dioxide	0.7	0.1–1.0
Oxygen	0.02	0.01–0.1
Hydrogen	Trace	Trace to 0.02

In the 21st century, the engine combustion is being practiced with low carbon dioxide emission. So natural gas is playing the important role to drive this clean energy

demand globally and becoming the biggest share among other fossil fuels toward the primary energy in 20 years. Even though big capacity of natural gas production is extracting from conventional reservoirs, it is still very active innovation to access unconventional deposits like coal bed, shale gas, tight gas, and hydrates to fulfill the projection of continued global demand at a growth rate about 2% until 2040 because of carbon-constrain and technology replacement (Veluswamy *et al.*, 2018).

2.2 Natural Gas Hydrates

Hydrates are parts of compound clathrates after the Latin word “clathrates” referring to “encage”. A gas hydrate is a solid ice-like formation of physical water bones, which is possible to trap guest gas molecules in its cavities. Many gases are possible to form hydrates under different conditions of temperatures and pressures, which drive to form three-dimensional shape of the host cavity (Chatti *et al.*, 2005). So, the guest gas can be encaged according to its molecule diameters, such as methane, ethane, hydrogen, nitrogen, carbon dioxide etc.



Figure 2.1 Methane gas hydrate sample (Demirbas, 2010).

First, Sir Humphry Davy (1810) conducted the experiment of an aqueous solution of chlorine, and found solid formation below 9 °C, but this type of solid was not recognized as a hydrate. It was just confirmed nearly 1 part of chlorine and 10 parts of water composite by Faraday. At the early age of hydrates, it was first interesting only by academic for what species and conditions (pressure, temperature) could form hydrates. Until 1934, the oil and gas industries were increasing rapidly in the US, Hammerschmidt reported the solid plugged in the natural gas pipeline due to solid ice-formation inside the pipes. To deal with gas pipeline clogged, industries, academic,

and researcher had tried actively to understand the condition of its formation and developed the statistical thermodynamic model for hydrate solid solution. After big thermodynamic data were developed in the 1960s, natural gas clathrate hydrates were recognized as natural occurrences with the very huge amount under the earth's crusts (Englezos, 1993).

This underneath natural gas hydrates were discovered approximately 1.5×10^{16} m³ in both offshore and on land, regarded as the potential reserves of gas for future development, Figure 2.2. Now people know that hydrate exists in nature since it worked an important role during formation planets and atmosphere and hydrosphere of the earth. However, gas hydrate deposit (GHD) were explored and understood as an unconventional reservoir, which would need advanced technologies to access for humankind. So, in the early 21st century, the productions of natural gas from GHD have encountered problems that made researchers and many countries like USA, Japan, India, China, Korea, and Germany set their own national program for studying hydrates. As the result, an example of natural gas production from GHD was produced from Siberia, in the northwestern part of Yakutia, well-heads Markhinskaya, where it was drilled down to 1,830 m in 1963. The condition of rock matched to temperature and pressure of hydrate formation by observing 0 °C temperature at a depth of 1,450 m and ending this permafrost at approximately 1,400 m. Soon after that, a group of young geologists found a real gas hydrate deposit in the Messoyakha field, at the western border of Siberia, where stable thermodynamic of natural gas hydrate deposits in the nature have been observed (Makogon, 2010). Moreover, the invention has been attempted to form gas hydrates for purposes of gas industries such as Marine CO₂ sequestration, separation process, coal storage application, and natural gas storage and transportation (Chatti *et al.*, 2005).

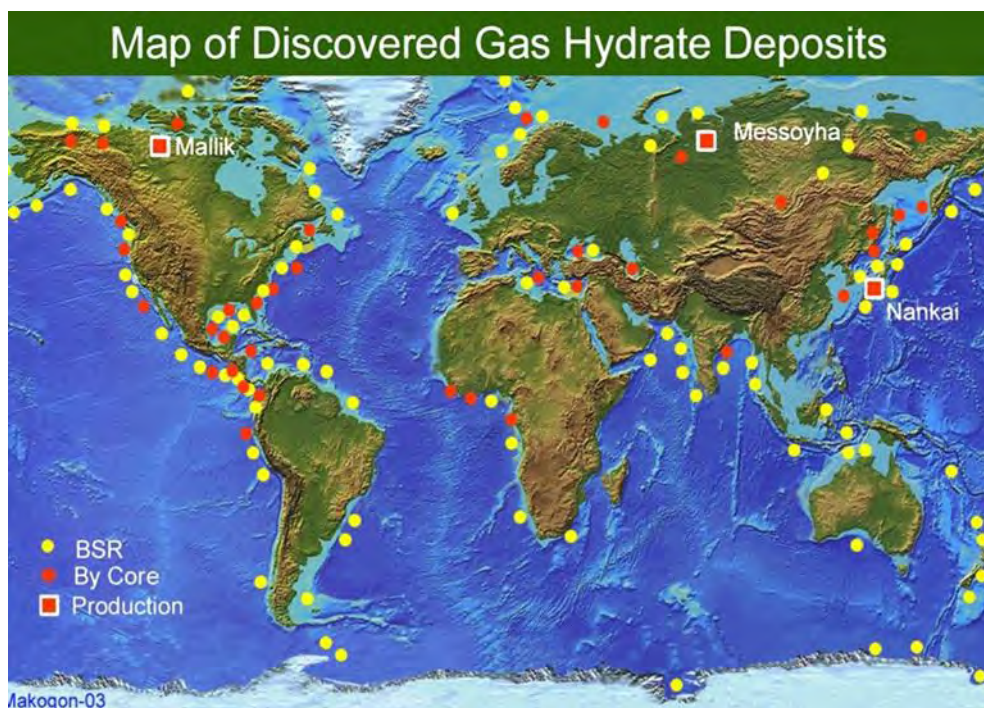


Figure 2.2 Distribution of discovered gas hydrate deposits. BSR¹/₄ deposit located by seismic refraction (Makogon, 2010).

2.3 Gas Hydrate Structures

Gas hydrates are known-stoichiometric compounds formed crystallized structures, where a guest gas molecule is small enough to be engaged by a well-defined diameter of hydrogen bonds of water molecules as in Figure 2.3. It is not chemical compound bonding, just made by a guest gas molecule inside the cage interacts with water via physical bonding, Wan de Waals force.

Therefore, the guest gas properties are not changed in the phenomena of hydrate formation and dissociation (Veluswamy *et al.*, 2018). There are three common structures of gas hydrates, namely sI, sII, and sH. These three well-known crystalline structures depend strongly on guest gas species, temperatures, and pressures; however, researchers found the others, nearly 10 structures at a high pressure above 100 MPa (Loveday and Nelmes, 2008).

In all three structures, there is only one guest gas molecule to be engaged typically, within one host cavity. However, multiple-cages occupancy occurred at

unusual conditions like high pressure. For example, of hydrogen hydrates at very high pressure form as many as two occupants in a small pore and four occupants in a large pore cage. In a particular sense, assume that all three type cavities are filled with guest molecules, their concentrations of components are approximately similar, 85 mol% water and 15 mol% guest(s) (Sloan, 2003).

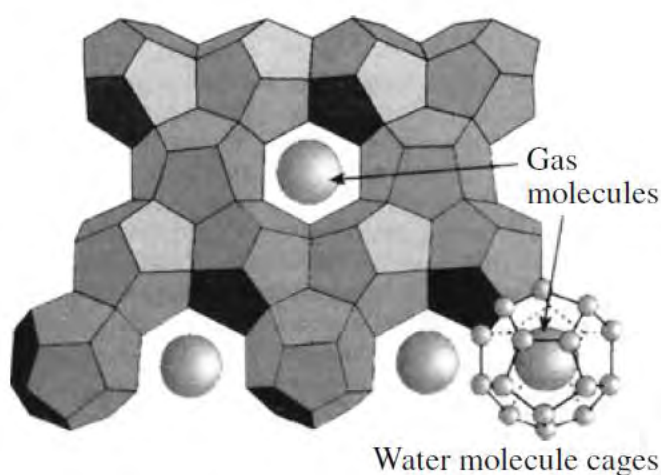


Figure 2.3 Water-ice-like cage structure (Demirbas, 2010).

The three common structures that occur at low temperature and moderate pressure compose of the polyhedral geometry of hydrogen bonding with water molecules, Figure 2.4. In addition, this single cage that is formed by polyhedral could contain one guest molecule per each and reach stable condition by physical forces van de walls, and repulsion forces of encaged molecules (Sloan and Koh, 2007).

Moreover, there are five types of polyhedral cages that are attached by hydrogen bonds of water molecules in order to form each three structural cavities (sI, sII, sH), (a) pentagonal dodecahedron (5^{12}), (b) tetrakaidecahedron ($5^{12}6^2$), (c) tetrakaidecahedron ($5^{12}6^4$), (d) irregular dodecahedron ($4^35^66^3$), and (e) icosahedron ($5^{12}6^8$), Table 2.2 and Figure 2.5

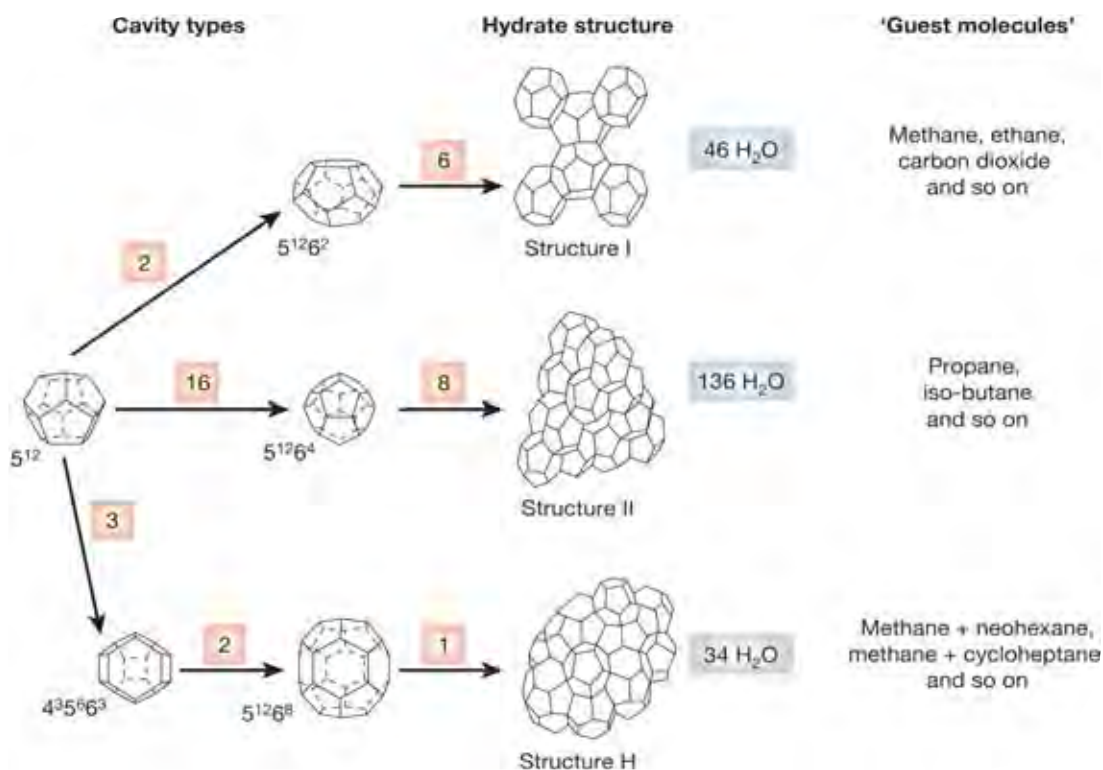


Figure 2.4 Three common hydrate structure compositions (sI, sII, sH) with water cage types that create hydrate structures (Sloan, 2003).

Table 2.2 Properties of three common unit crystals (Sloan, 2003)

Hydrate crystal structure	I		II		H		
	Small	Large	Small	Large	Small	Medium	Large
Cavity	5 ¹²	5 ¹² 6 ²	5 ¹²	5 ¹² 6 ⁴	5 ¹²	4 ³ 5 ⁶ 6 ³	5 ¹² 6 ⁸
Description							
Number of cavities per unit cell	2	6	16	8	3	2	1
Average cavity radius (Å)	3.95	4.33	3.91	4.73	3.91 [†]	4.06 [†]	5.71 [†]
Coordination number*	20	24	20	28	20	20	36
Number of waters per unit cell	46		36		34		

*Number of oxygens at the periphery of each cavity.

[†]Estimates of structure H cavities from geometric models.

The cage size and shape interpretation are as following: pentagonal dodecahedron (5¹²) is classified in small cage type (S), irregular dodecahedron (4³5⁶6³) is medium (M), and tetrakaidecahedron (5¹²6²), tetrakaidecahedron (5¹²6⁴), and icosahedron (5¹²6⁸) are large (L), Table 2.2 (Sloan and Koh, 2007).

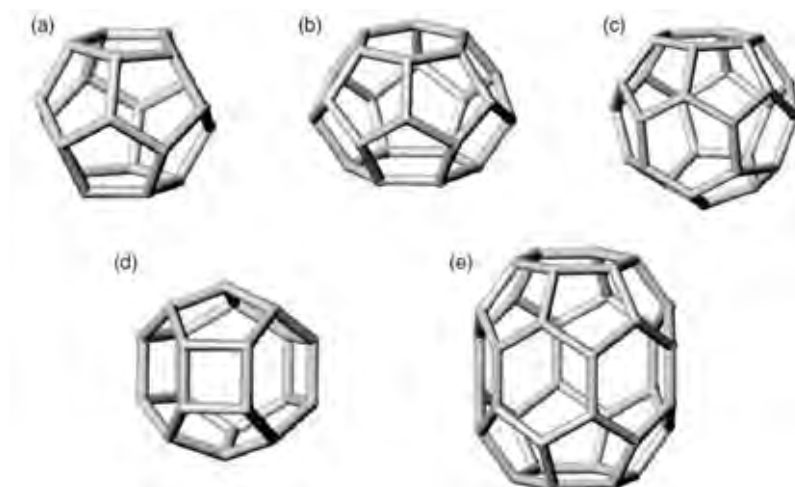


Figure 2.5 Different five cages that form each three structures: (a) pentagonal dodecahedron (5^{12}), (b) irregular dodecahedron ($4^35^66^3$), (c) tetrakaidecahedron ($5^{12}6^2$), (d) tetrakaidecahedron ($5^{12}6^4$), and (e) icosahedron ($5^{12}6^8$) (Sloan and Koh, 2007).

2.3.1 Structure I (sI)

The structure I is called the simplest crystal structure, which is commonly observed in the earth's natural environment and shape cubic structure. Guest gas molecules are particularly engaged a small diameter (0.4-0.55 nm) in each cavity. Basically structure I composes of two cavity types, by two pentagonal dodecahedrons (5^{12}) and six tetrakaidecahedrons ($5^{12}6^2$), Figure 2.6, with forty-six water molecules to arrange per unit cell, which is possible to accommodate eight guest gas molecules, approximate 5.8 Å in diameter. The included gaseous molecules are formed by smaller molecules, likely methane, ethane, carbon dioxide (Demirbas, 2010; Sloan, 2003).

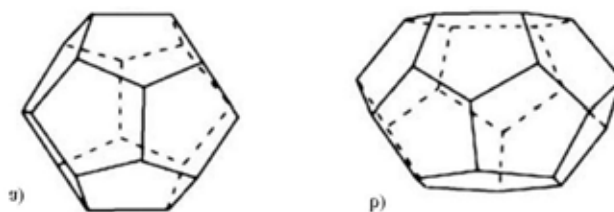


Figure 2.6 Gas hydrate of structure I composes of two pentagonal dodecahedrons (5^{12}), and six tetrakaidecahedrons ($5^{12}6^2$), figure a) and b), respectively (Demirbas, 2010).

2.3.2 Structure II (sII)

A hydrate structure II has more complex crystal structure than structure I, which composes of 136 water molecules per cubic unit cell. However, this unit cell contains the combination of large and small cages of eight hexakaidecahedrons ($5^{12}6^4$), the diameter of 3.92 Å and sixteen dodecahedrons (5^{12}), the diameter of 4.73 Å, respectively Figure 2.7, which can host twenty-four guest molecules, approximate up to 6.9 Å in diameter. The inclusion of gas molecules is a bit larger than those gases in structure I, such as propane and isobutene. Both sI and sII are the most stable hydrate structures, which are possible to fill at least up to 75% of its cavities by single guest molecules (Demirbas, 2010).

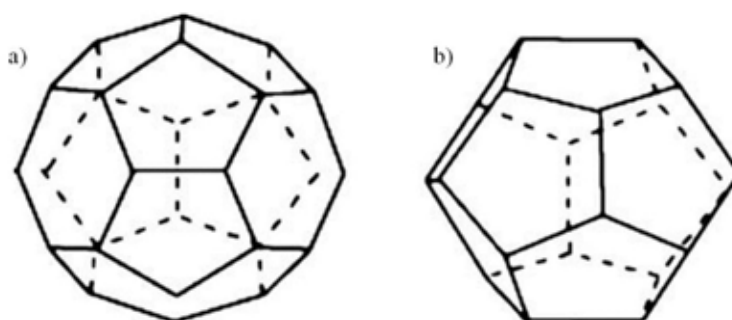


Figure 2.7 Gas hydrate of structure II, a) hexakaidecahedron and b) dodecahedron (Demirbas, 2010).

2.3.3 Structure H (sH)

Structure H composes of thirty-six water molecules and forms a hexagonal unit cell by arranging three pentagonal dodecahedral voids (5^{12}), two irregular dodecahedral voids ($4^35^66^3$), and one icosahedral void ($5^{12}6^8$), Figure 2.8, which is possible to host even larger guest gas molecule. A noticeable aspect of sH is that two sizes of molecules are required to stabilize this structure. Series of small molecules, likely methane or hydrogen sulfide, stay in both small cavities (5^{12} and $4^35^66^3$) and large molecules typically larger than 7.3 Å, such as 2,2-dimethylbutane (neohexane), stay in the ($5^{12}6^8$) cavity. Unlike structure I and II, which commonly form hydrates readily with single occupants of either the small and/or large cavity (Demirbas, 2010; Sloan and Koh, 2007).

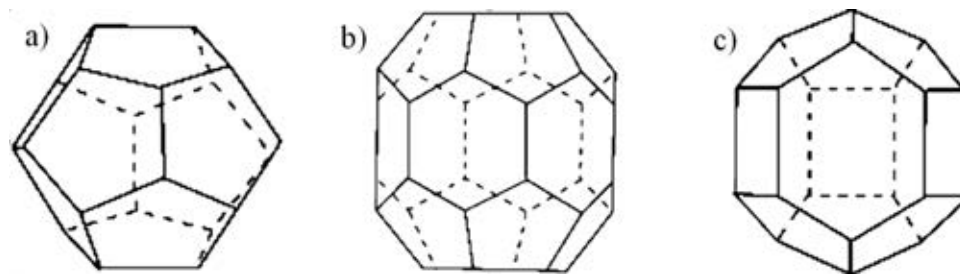


Figure 2.8 Gas hydrate of structure H, a) pentagonal dodecahedron, b) icosahedron, and c) irregular dodecahedron (Demirbas, 2010).

Structure H is not a common hydrate formation in earth's natural environment and was not frequently seen since this specific formation needs guest gas molecule, methane, to help link the lattice to form structure. In other words, it was rarely observed in the natural gas experiment; but, structure I and II prefer to occur with natural gas (Carroll, 2004).

2.4 Gas Hydrate Formation Processes

Last decade, the most challenging and intriguing questions regarding hydrate formation and dissociation phenomena were not well understood. As in Figure 2.9, the curve of gas consumption vs time is a remarkable example of gas hydrate phenomena to form a solid structure. The study took place in an agitated system, where temperature and pressure were kept constant. First, an autoclave cell with water inside was pressurized with a gas injection to the reservoir and brought hydrate formation in a low-temperature water bath. Then gas was introduced from the reservoir to the crystallizer cell to observe the hydrate formation with time recorded. Afterwards, the constant pressure of the gas was known to be consumed by hydrate formation rate, which could be controlled by the kinetics, or heat, or mass transfer (Sloan and Koh, 2007).

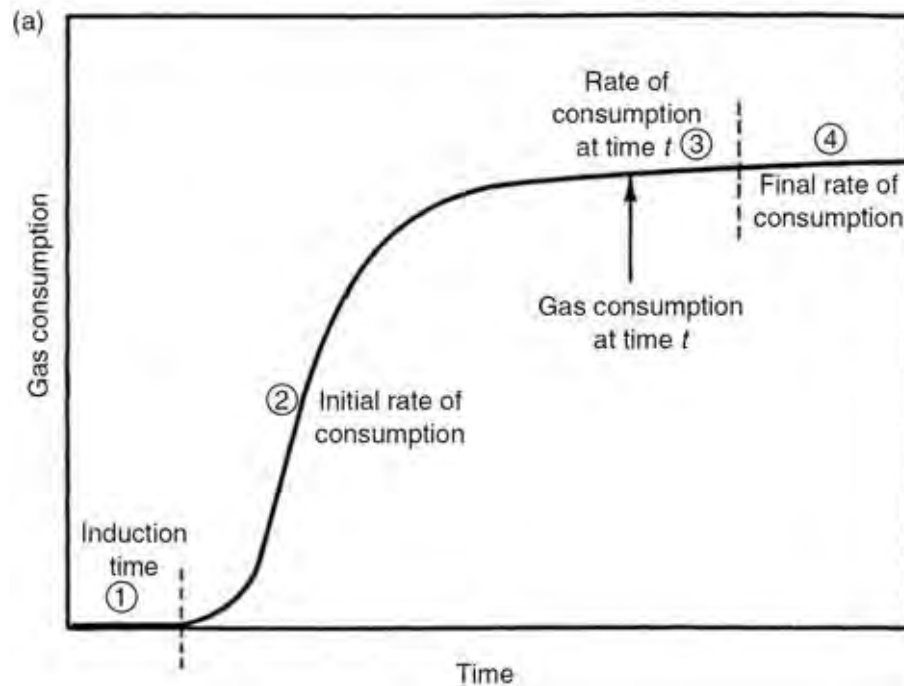


Figure 2.9 Curve of gas consumption and time for hydrate formation (Sloan and Koh, 2007).

A marked number 1 is called induction time that was recorded since the gas was introduced to the crystallizer cell till the minimum of solid formed. In other words, induction time or hydrate nucleation is defined as the time taken until the appearance of a detectable volume of hydrate phase. During this period, temperature and pressure are still stable in the region without any hydrate formation because of metastability, which is the ability to keep non-equilibrium state to persist for a long period of time. Region number 2 is called hydrate growth where hydrates start suddenly to grow. This period, the gas is being concentrated by encaging into the water cavities. As the water molecules are being consumed by hydrate formation, the gas consumption slope raises accordingly to the time, region 3 and 4 (Sloan and Koh, 2007).

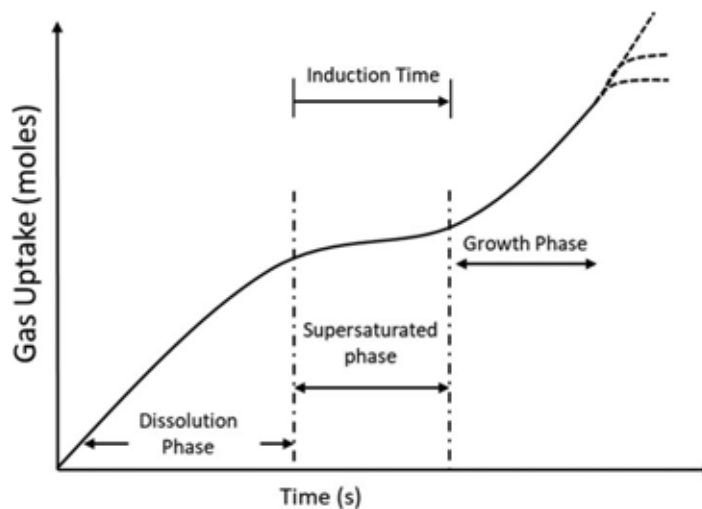


Figure 2.10 Hydrate formation schematic represented by gas uptake in an experiment vs time showing three main phases in hydrate formation process: dissolution phase, supersaturated phase, and growth phase (Khurana *et al.*, 2017).

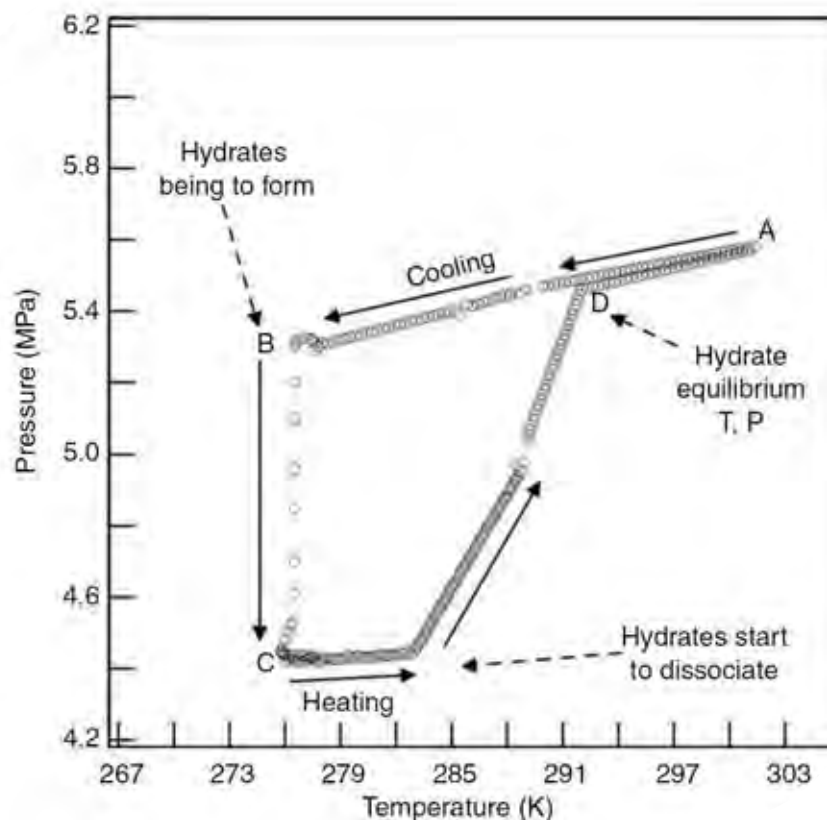


Figure 2.11 Temperature and pressure trace for formation of simple methane hydrates (Sloan and Koh, 2007).

According to Khurana *et al.* (2017), the different stages for the process of hydrate formation is observed in Figure 2.10. Normally guest molecules present in the gas phase which is introduced to host molecules, liquid water. Then the process starts with the increasing of gas uptake due to gas dissolution into the bulk water. After this stage, the supersaturation phase begins when the thermodynamic condition (T, P) favors the formation of hydrates but the appearance of critical hydrate nuclei.

A critical nucleus of a hydrate phase could be defined as a new phase in a system, which is capable of existing independently. The period, which is between supersaturation and a formation of critical nuclei, is called induction time. However, reaching supersaturation is not guaranteed that a critical nucleus and hydrate formation have to occur. The hydrates grow process is followed by the catastrophic growth with increasing rapidly the gas uptake. Finally, the process of hydrate reaches the different level of gas uptake depending upon the mass transfer resistance and final hydrate formation by the dotted trajectories (Khurana *et al.*, 2017).

Figure 2.11 illustrates the temperature and pressure profiles during the hydrate formation process. Point D is a metastability that prevents the rapid hydrate formation in equilibrium temperature and pressure. From A to B, the pressure and temperature are decreasing linearly without hydrate formation for a number of hours, It is actually an induction time period. At point B, the hydrate starts to grow, that could be observed that pressure drops rapidly to point C, namely catastrophic grow period (Sloan and Koh, 2007).

2.4.1 Hydrate Nucleation

Hydrate nucleation is the process, by which a small cluster of water and gas grows and disperses in the attempt to form the critical size for continuing growth, involving ten to thousands of molecules. The solubility of nonpolar gases in liquid water is very small, at pressures both above and below the hydrate formation point (Sloan and Koh, 2007).

Nucleation process was typically found in two types. Firstly, homogeneous nucleation is the nucleus of the hydrate phase emerging directly from the parent phase. It is generally observed in systems without any impurities and considered to be stochastic in nature. Secondly, heterogeneous nucleation nucleates in

contact with a third phase, which can be either foreign particle or surface. In terms of system free energy, it is more favorable to form hydrates on a two-dimensional surface than a three-dimensional nucleus in the bulk water phase. The presence of a third phase lowers the interfacial energy necessary to overcome in nucleation phenomenon. Hence, heterogeneous nucleation is more rapid than homogeneous nucleation, and the critical radius for nucleation is less than homogeneous. However, in practical conditions, hydrate nucleation through homogeneous nucleation is very unlikely and proceeds through heterogeneous nucleation (Khurana *et al.*, 2017).

It was found that hydrates usually occur at the interface between vapor and liquid water within a thin film because it is not only that the interface has lower interfaces Gib free energy of nucleation, but this location is also a high concentration of host and guest molecules. In contrast, the bulk water contains lower guest component concentration that causes to form the nuclei, so hydrate formation is unlikely to form in bulk phase (Sloan and Koh, 2007).

There has been a general researchers' agreement that hydrates retain a "memory" of their structure when melted crystal body at moderate temperatures. Consequently, hydrates form more easily from gas and water obtained by melting hydrates than from fresh water with no previous hydrate history. Conversely, if the hydrate system is heated sufficiently above the hydrate formation temperature at a given pressure, the "memory effect" will be destroyed (Sloan and Koh, 2007).

2.4.2 Hydrate Nucleation Growth

Nucleation and crystal growth process are the analogous events, which appear respectively. The induction time in nucleation might take awhile to reach the maximum solubility; afterward, the crystal growth occurs rapidly.

Based on the Figure 2.12, a) the initial condition: pressure and temperature are introduced into the system, but no dissolution of gas molecules in the water yet, b) labile cluster: molecules of water and gas get altered together to form a suitable cavity size or forming a cluster, c) agglomeration: labile cluster moves to the others and sharing the same face to form an agglomerated cluster and d) primary nucleation and growth: growths begin when the size of cluster agglomerate reaches the critical value (Sloan and Koh, 2007).

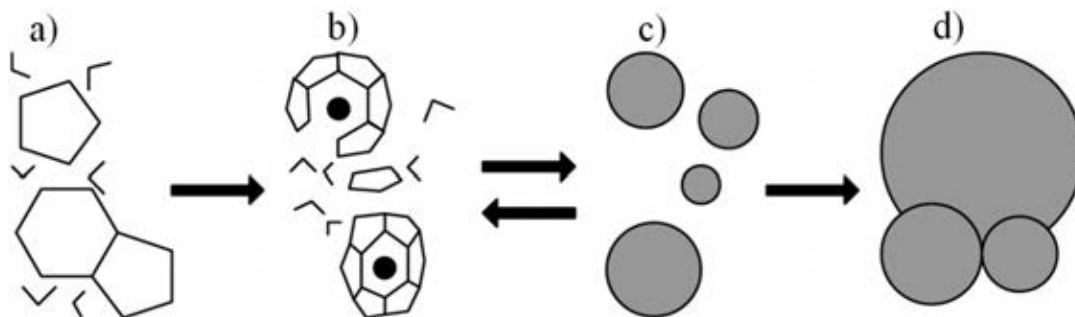


Figure 2.12 Schematic model of labile cluster growth: a) the initial condition, b) labile cluster, c) agglomeration, and d) primary nucleation and growth (Sloan and Koh, 2007).

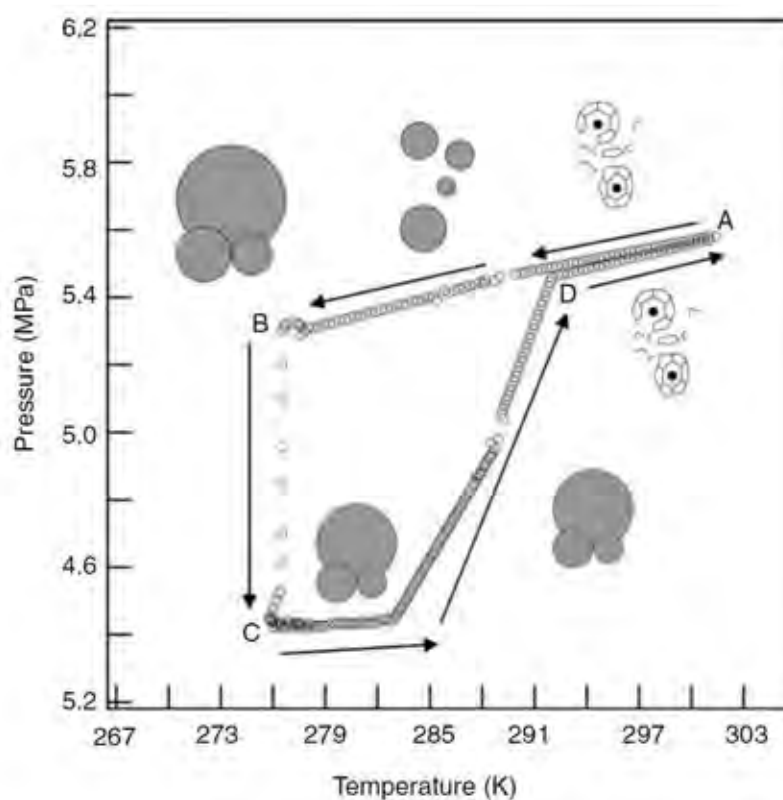


Figure 2.13 Hydrate labile cluster growth mechanism imposed on a pressure-temperature trace (Sloan and Koh, 2007).

Figure 2.13 illustrates the cluster mechanism that imposes on the pressure-temperature trace. At point A after pressurization of the system, guest molecules are dissolved in water and short-lived cages have been formed. The linkages of clusters to each other occurs after cooling from point A until a critical radius cluster is formed at point B, where catastrophic nucleation and growth occur. If heating the system from point C, the reaction is driven to dissociate the hydrate crystal and release guest gas molecules (Sloan and Koh, 2007).

However, on the molecular scale, hydrate crystal growth could be considered to be a combination of three factors: (1) the kinetics of crystal growth at the hydrate surface, (2) mass transfer of components to the growing crystal surface, and (3) heat transfer of the exothermic heat released away from the growing crystal surface. There are four types of crystal growth process (1) single crystal growth, (2) hydrate film/shell growth at the water-hydrocarbon interface, (3) multiple crystal growth in an agitated system, and (4) growth of metastable phases. But in this reveal, type (1) and (2) are particularly highlighted (Sloan and Koh, 2007).

Single crystal growth: this typical growth mostly occurs at lower driving force conditions. For an instant, the observation on additive of tetrahydrofuran (THF, sII hydrate) and ethylene oxide (sI hydrate) as in Figure 2.14, these two cases have been studied the morphology of hydrate formation, regarding hydrate formation occurs at the higher freezing point of water, ambient pressure, and high additive soluble in water. The single crystal growth with tetrahydrofuran is within the plan (110), forming structure II (sII), and a single crystal with ethylene carbon dioxide form within the plan (111), in structure (sI) (Sloan and Koh, 2007).

Hydrate film/shell growth at the water-hydrocarbon interface: this kind of crystal growth, the water and hydrocarbon interface change generally the morphological condition regardless of the same hydrate formers. Normally hydrate nucleation and growth start initially at the interface between hydrocarbon and water. Because the saturation (or the driving force) has an effect on morphology, and the observation has been noticed that the similarities between growth behavior at a water hydrate former planar interface and at the surface of a liquid droplet (Sloan and Koh, 2007).

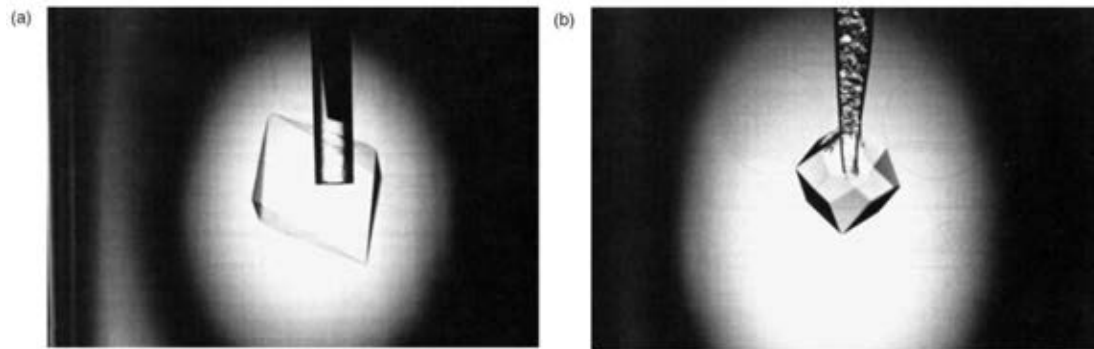


Figure 2.14 Photograph of single hydrate crystals of (a) tetrahydrofuran (sII); (b) tetrahydrofuran (sI) (Sloan and Koh, 2007).

Based on the experiment made by Servio and Englezos (2003), the hydrate growth with driving force applied to the system consists of three growth phases 1) the appearance of minor hydrate layer (shell), around the water droplet with needle-like crystals, and up to 10 h after nucleation the needle-like crystals grow in size and thickness, 2) the disappearance of needle-like crystal, instead of appearance of hydrate layer covering the droplet, and 3) the appearance of depression in the hydrate layer surrounding the water droplet, which took approximately 10-15 h or over a couple of days in some experiments.

Figure 2.15a, while at the high driving force of pressure in the system, the crystal hydrate was observed, but, at low driving forces, there was no sight of crystal hydrate on the surface, Figure 2.15 b. That was a reasonable claim proved the higher driving forces produced a great number of core elements area compared to lower driving force. Mullin (2001) also reported the rate of nucleation depend on the number of nuclei form per time per unit of volume, which was dramatically increasing with the degree of supersaturation. The driving force is a relation proportionally to supersaturation that means where there is a higher driving force. As the result, there are randomly crystal growths and a rougher surface in the observation (Sloan and Koh, 2007).

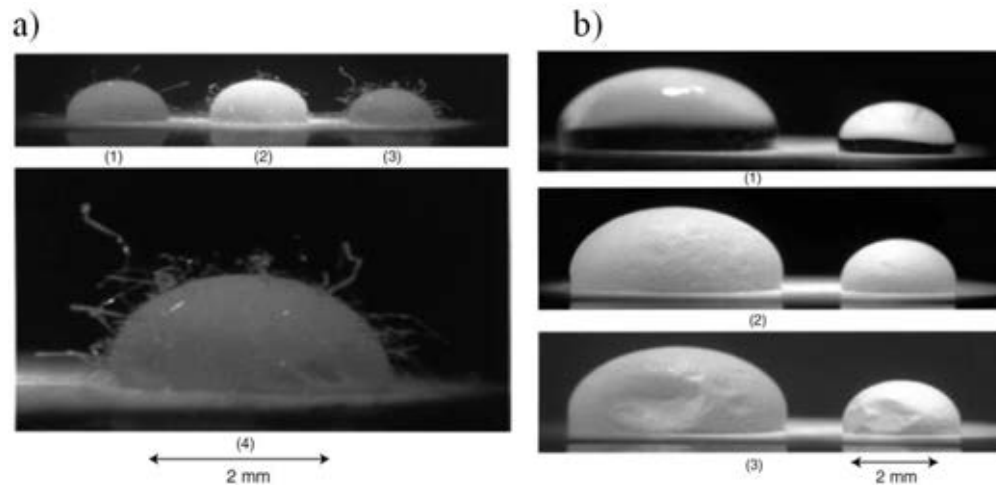


Figure 2.15 a) Methane hydrate covering the surface of water droplets (1, 2, 3) under high driving force, 10 min after nucleation. Image (4) is a magnified view of droplet (3), and (b) methane hydrate covering two water droplets under low driving force at three different times: (1) at $t = 0$, (2) at $t = 10$ h where the water droplet is covered by hydrate, (3) at $t = 25$ h where the water droplet is covered by hydrate and depressions in the hydrate layer appear (Servio and Englezos, 2003).

2.4.3 Hydrate Equilibrium

In nature, gas hydrates are stable under suitable thermodynamic conditions, likely low temperature and high pressure. Frequently, natural gas deposits are not in place within the same character models, because each marine environment builds up with the different geological formation at underneath. The stability of hydrate deposit zones is incorporated with the water depth, seafloor temperature, geothermal gradient, and local pressure. However, if any change to temperature, pressure, and geological parameters in the hydrate deposits, there would be effects on the stabilization zone. In addition, even temperature and pressure are the main influence factors of hydrate formation and thickness of stability zone, the other disturbances such as gas compositions and gas chemistry also alter the location of the stabilized zone (Nixon and Grozic, 2006).

According to Clennell *et al.* (1999), hydrate stability occurs only in the right position if there is not too deep beneath the sea level and high enough pressure. In contrast, if there is not found hydrate stability, it could involve with inhibitor

mechanism, as in Figure 2.16. Methane hydrate stability curve with pure water moves upward beyond methane with seawater curve.

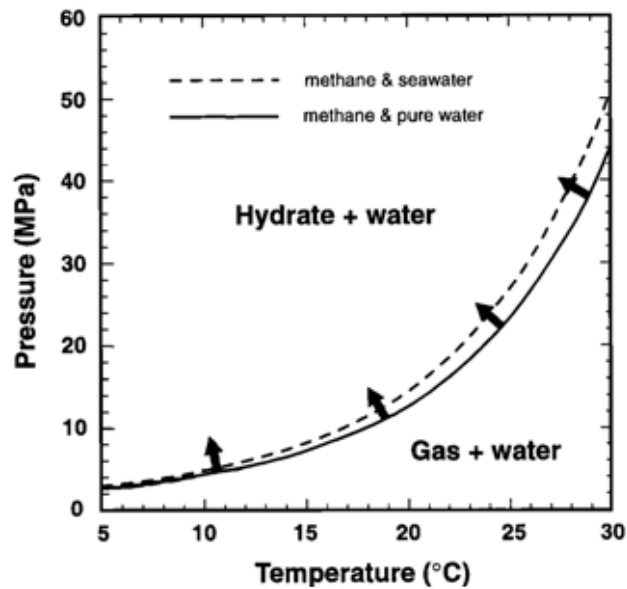


Figure 2.16 Diagram of stability with assuming methane-pure water and methane seawater (Clennell *et al.*, 1999).

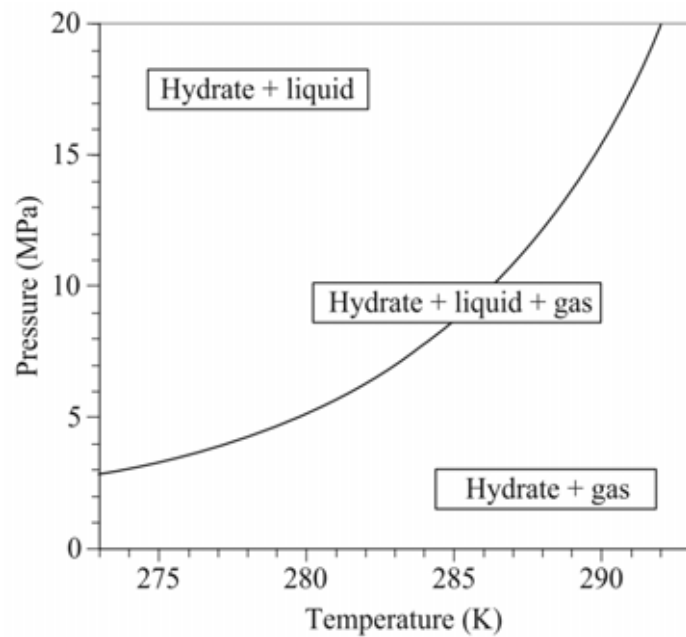


Figure 2.17 Phase equilibrium diagram for methane hydrate diagram for methane hydrates (Demirbas, 2010).

Figure 2.17 demonstrates the phase equilibrium for methane hydrates. The temperature and pressure, that is outside the hydrate stability zone, will cause melting and decompose hydrate formation, so the volume of methane gas and liquid water will be released separately. The decomposition of hydrates could be stem from the changes of pressure and temperature regime in the stable zone. In addition, the distance from equilibrium conditions is assumed as a driving force for hydrate formation. Therefore, the equilibrium curve represents the temperature and pressure condition where the hydrate decomposes (Demirbas, 2010).

2.5 Gas Hydrate Dissociation

Hydrate dissociation was first the only techniques, which have been used to deal with plugging pipes in the oil and gas industries. Later on, clathrate hydrates were found in an abundant permafrost and subsurface and attempted to include into gas storage and transport technology, the dissociation process becomes an importance. It is an endothermic process that reserves the from exothermic hydrae formations. Therefore, the dissociation process will be supplied amount of heat to break the hydrogen bonds between water molecules and Van de Waals interaction force of guest gas molecules (Sloan and Koh, 2007).

There are three techniques available to conduct the dissociation process, Figure 2.18, thermal injection, depressurization, and inhibitor injection. Thermal stimulation has been developed by doing in a computer model to evaluate the production of natural gas from hot water and steam floods and gained technically in a sufficient rate of recoverable resources, but it was prohibited in terms of economic. Similarly, inhibitor injection has been used in the production of gas from hydrate deposits and shown to be technically feasible; but the very huge amount of chemicals such as methanol and glycol would cost over making a profit. Therefore, among technical approaches, depressurization might be a priority to produce gas from in-situ hydrates (Collett, 2002).

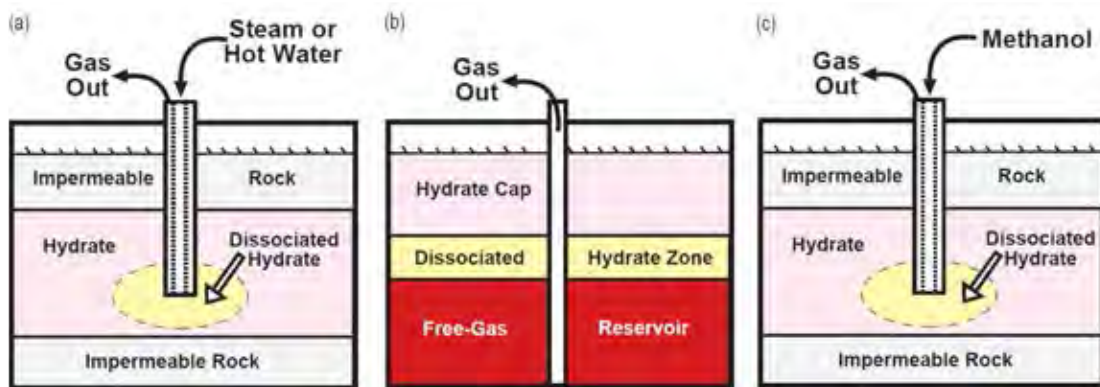


Figure 2.18 Schematic of proposed gas hydrate production methods: (a) thermal injection; (b) depressurization; (c) inhibitor injection (Collett, 2002).

The blockages of hydrates in the petroleum and gas industries is a normal concern, which enhances the discovery of hydrate dissociation techniques. According to Koh (2002), the thermodynamic inhibitor has been used to prevent the formation of hydrate in a pipeline by generally injecting a high concentration of 40 vol% methanol. This typical inhibitor was operated to shift the phase of hydrate formation boundary away from pressure and temperature of hydrate formed, by increasing the driving force required, Figure 2.19. In general, thermal stimulation has been seen frequently in small-scale applications by heating the water circulation in a water bath, likely dissociation of gas hydrates' experiment. There was a report that the self-preservation phenomena interrupts the process of hydrate decomposition. Self-preservation leads the crystal hydrates to remain stable for extended periods even out of the stability region.

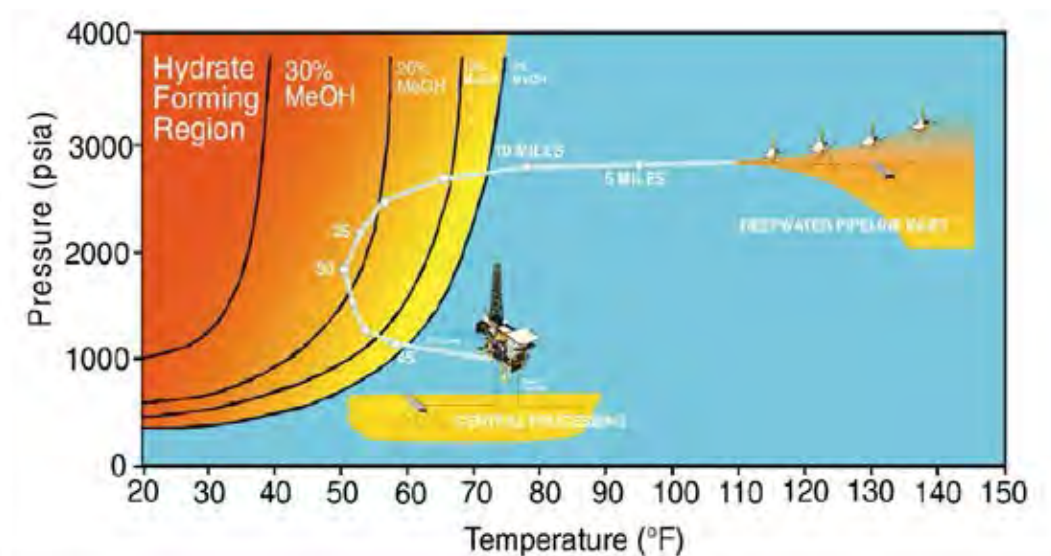


Figure 2.19 Diagram of the phase boundary of methane hydrate formation as a function of temperature pressure with water depth (Koh, 2002).

2.6 Hydrate Promoters

Since gas hydrates have been not well-known globally and first presented in the US transmission system of the natural gas pipeline, Hammerschmidt (1934) reported that they were a solid ice plug problem. Latter on, the drawbacks of compound clathrates were reported as a new possible approach for gas storage technology that gained attraction. However, the attempt to produce large scale of solidified natural gas (SNG) for storage and transport is much development with the slow formation kinetics as the main issues (Veluswamy *et al.*, 2018). Hence, the enhancement was proposed to speed up the formation by using additive compounds.

2.6.1 Kinetic Promoters

Hydrate kinetic promoters are the additives, which enhance the rate of hydrate formation effectively, without any influences the thermodynamics. Thus, hydrate formation will be formed within unchanged temperature, pressure, and hydrate structures.

Surfactant: first methane hydrate formation with a series of surfactants was performed by (Kalogerakis *et al.*, 1993). A preferable kinetic promotion was

announced that surfactants altered significantly the surface or interfacial free energy, by forming a colloidal-size cluster in the solution called micelles. An effective anionic surfactant, sodium dodecyl sulfate (SDS), and three non-ionic surfactants were investigated and reported the effects to create kinetic. SDS system was observed faster hydrate formation rate compared to other non-ionic surfactants (Veluswamy *et al.*, 2018)

The effects of surfactants on ethane and natural gas (90% methane, 6% ethane and 4% propane gas mixture) were investigated by Zhong and Rogers (2000). The results were found that the surface tension of the surfactant solution was altered significantly when surfactant concentration reached steady critical micelles concentration (CMC) and molecules of the surface associated as micelles. However, a remarkable alteration in hydrate formation rate of ethane and natural gas had been noted well below this CMC value. As in Figure 2.20, a faster kinetics of ethane hydrate formation with the presence of surfactant was shown compared to the non-surfactant system (Veluswamy *et al.*, 2018).

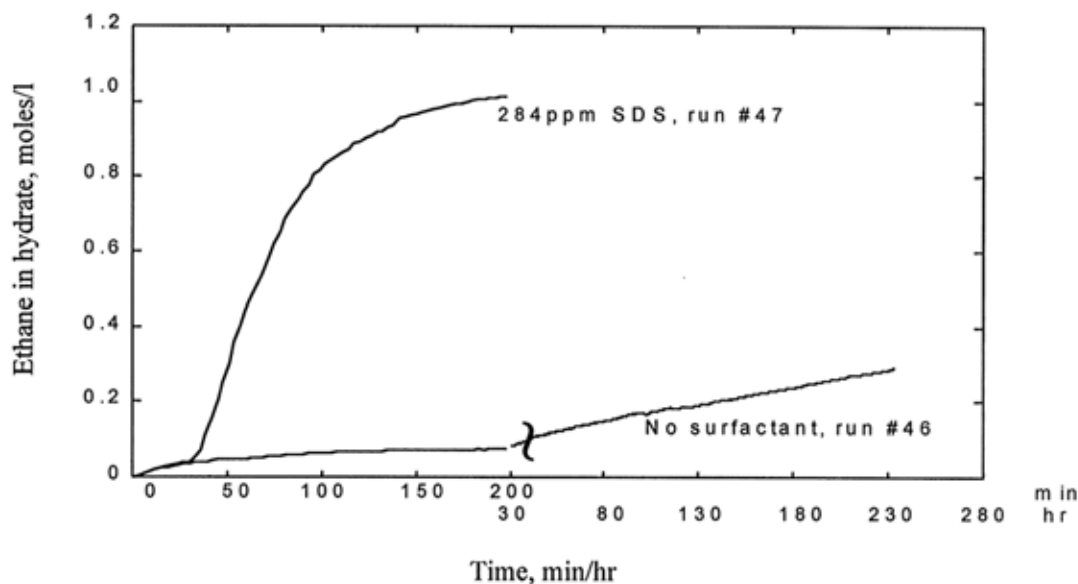


Figure 2.20 Surfactant increases formation rate, the quiescent system (Zhong and Rogers, 2000).

Polymers and Starches: Polymers have been investigated and reported their additives, which consisted of OH molecular structure, to accelerate the methane hydrate formation. On the other hand, among these OH polymers addition, a smaller molecule size has been reported as the most effective compared to the others (Karaaslan and Parlaktuna, 2002). Two polymers, poly-2-acrylamide-2-methylpropane sulfonic acid and polyacrylic acid, were observed to promote effectively methane hydrate formation kinetics at 0.5 wt% concentration at 6.5 MPa and 277.2 K (Karaaslan and Parlaktuna, 2002; Veluswamy *et al.*, 2018).

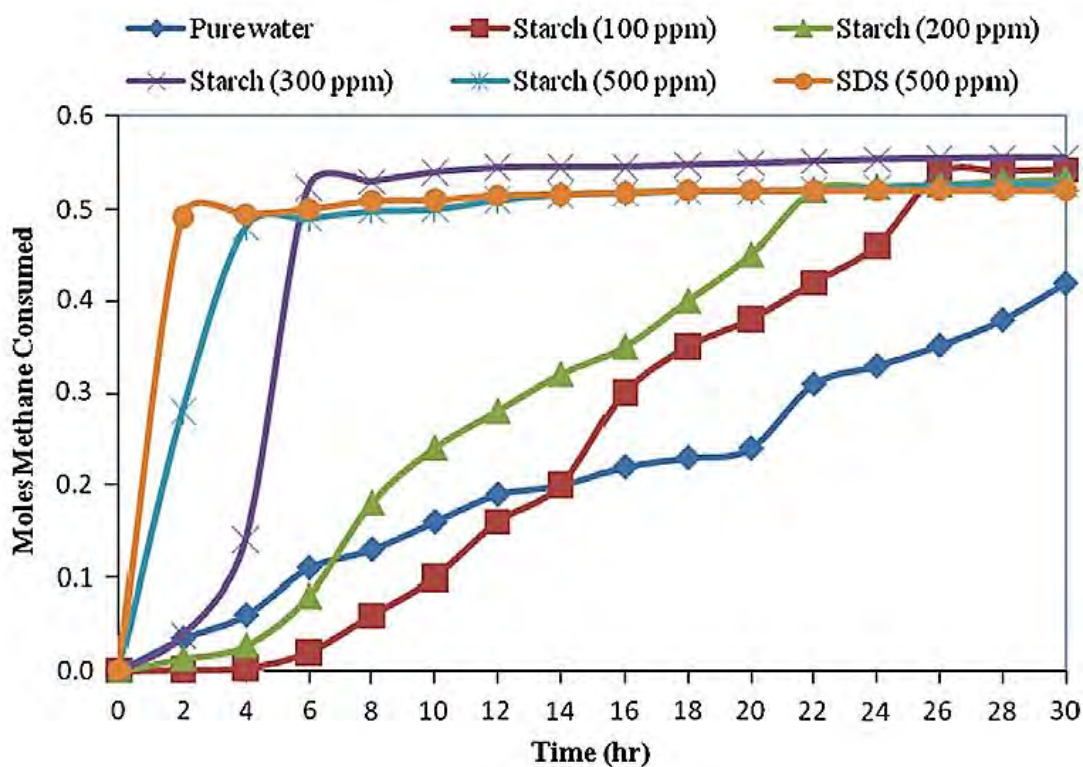


Figure 2.21 Methane hydrate formation rate with and without additives (Fakharian *et al.*, 2012).

The promotion effect of potato starch may be attributed to the phosphate groups in its molecular structure. These groups give anionic behavior to the solution and can enhance the water hydrogen bonding which leads to more stable cages. Based Figure 2.21, the starch in all concentration is possible to increase the hydrate formation

rate and gas consumption with slightly increasing the concentration respectively (Fakharian *et al.*, 2012).

Amino Acid: a serine amino acid was firstly involved with clathrate hydrates in the use for hydrate formation inhibitor. Recently Liu *et al.* (2015) found some amino acids, which consisted of an amine (-NH₂) and carboxylic (-COOH) functional group along with a characteristic side chain, promoted effectively the kinetics of hydrate formation. The promotion effects occurred because of their surface activity and surface adsorption at the water-gas interfaces.

A high methane uptake was reported by the addition of l-leucine amino acid with the methane uptake capacity of 141 mg/g (161.7 mmol of gas/mol of water). The effect of l-leucine at 0.5 wt% concentration could take 20 minutes to complete 90% of hydrate formation, at 9.5 MPa and 273K as in Figure 2.22 (Liu *et al.*, 2015; Veluswamy *et al.*, 2018).

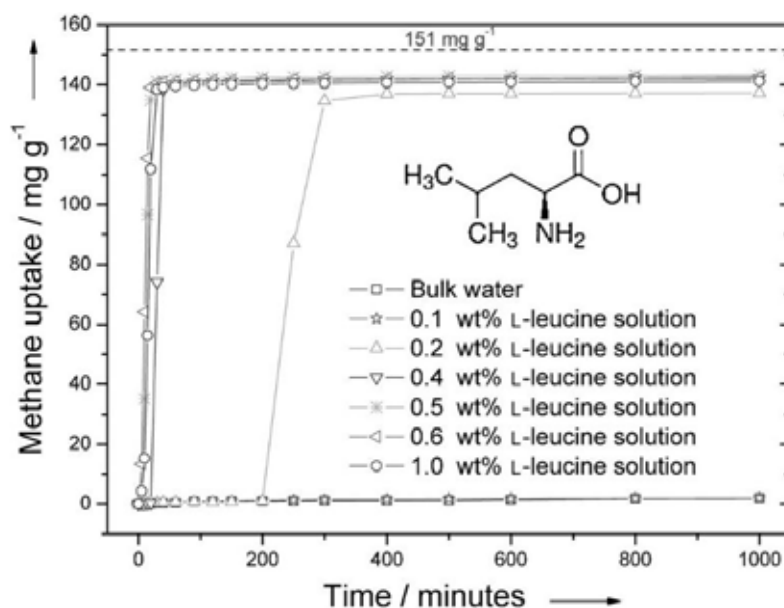


Figure 2.22 Methane uptake kinetics for bulk water and l-leucine aqueous solutions at 273 K (Liu *et al.*, 2015).

2.6.2 Thermodynamic Promoters

Thermodynamic promoters are the compound additive in order to form clathrate hydrates outside the equilibrium condition (lower pressure and higher temperature). Addition of thermodynamic promoter leads to lower energy requirement during hydrate formation, but the drawback of conduction with thermodynamic promoters is the obvious reduction in methane storage capacity due to the occupation and stabilization of large hydrate cages by promoter molecules themselves (Veluswamy *et al.*, 2018).

Thermodynamic effects were investigated by using tetrahydrofuran (THF), propylene oxide, 1,4-dioxane, and acetone were chosen and their concentration was fixed at 3 mol% relative to water. As the result in Figure 2.23, the best stabilization effects were found in the solution with THF, or likely THF > propylene oxide > 1,4-dioxane > acetone (Seo *et al.*, 2001).

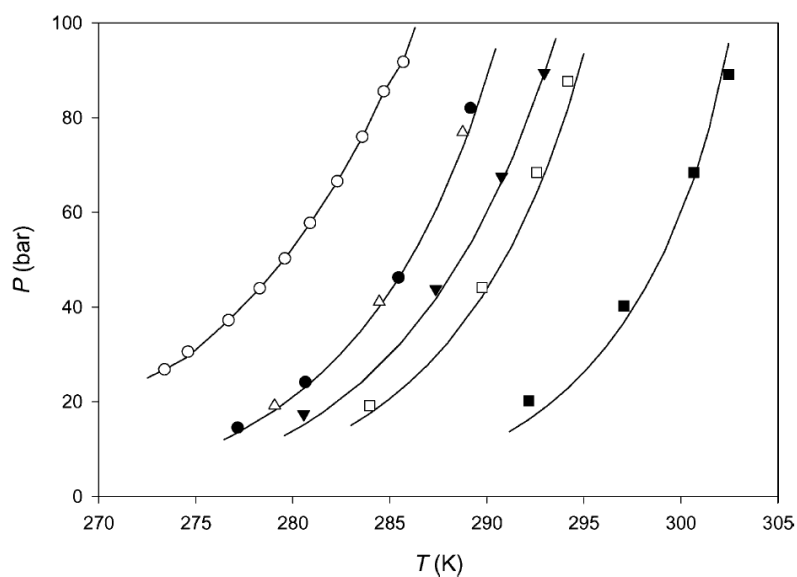


Figure 2.23 Experimental and predicted hydrate dissociation pressures for the binary and ternary systems of : (O) water + methane, (●) water + methane + acetone, (▼) water + methane + 1,4-dioxane, (□) water + methane + propylene, (■) water + methane + THF, (-) predicted (Seo *et al.*, 2001).

CHPATER III

EXPERIMENTAL

3.1 Materials and Equipment

3.1.1 Materials

- Amino acids (l-leucine, and l-valine)
- Surfactants (sodium dodecyl sulfate, and ethyl ester sulfonate)
- Ultra high purity methane gas
- Deionized water

3.1.2 Equipment

- Reservoir (R)
- Crystallizer (CR)
- Personal computer (PC)
- K-type thermocouples
- Pressure transducer (PT)
- Controllable water bath
- WISCO Software

3.1.3 Chemicals

- Ultra high purity methane (99.999% purity), from Labgaz Co., Ltd., Thailand
- L-leucine (reagent grade, 98% purity), from Sigma Aldric Pte. Ltd.
- L-methionine (reagent grade, 98% purity), from Sigma Aldric Pte. Ltd
- L-valine (reagent grade, 98% purity), from Sigma Aldric Pte. Ltd
- Sodium dodecyl sulfate (SDS)
- Methyl ester sulfonate (MES)
- Deionized water

3.2 Methodology

3.2.1 Experimental Schematic

An experimental setup, Figure 3.1a, composed of stainless steel crystallizer (CR), and a supply gas reservoir (R). Both the reservoir and crystallizer were immersed in the cooling water bath, the temperature of which is monitored and adjusted by the internal controllable circulator. Two pressure transducers were connected to the gas stream and measure the pressure in the system.

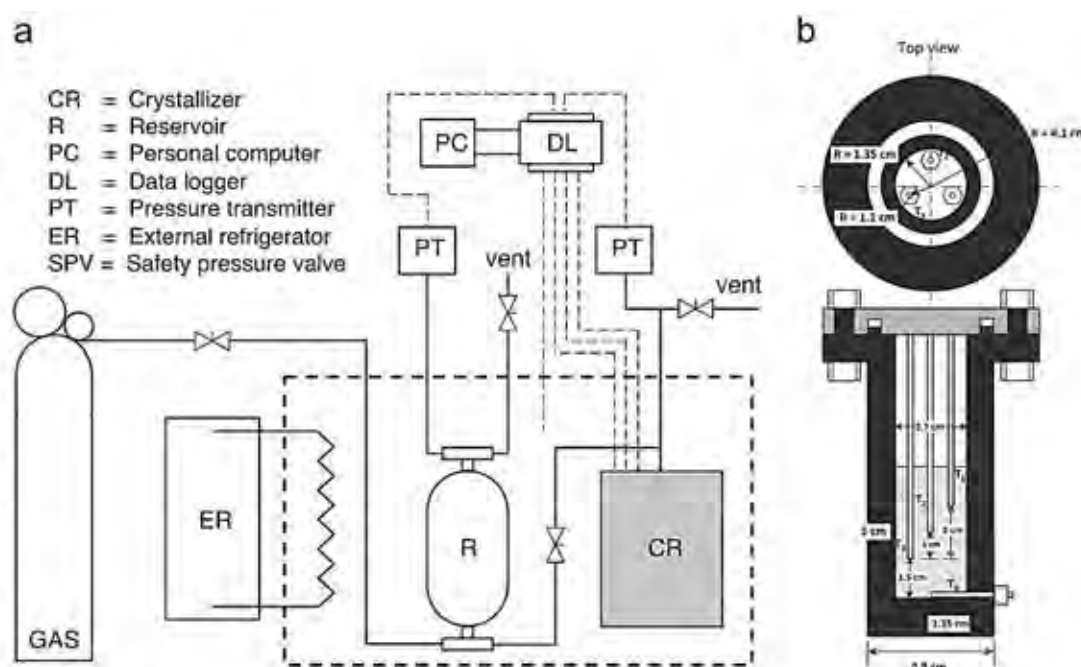


Figure 3.1 Schematic diagram of gas hydrate apparatus; a) schematic diagram, b) cross-section of a crystallizer (Siangsai *et al.*, 2015).

A data logger was connected to a personal computer to record data of forming and dissociation hydrates. The temperature data was recorded by four K-type thermocouples, which were at different positions in the crystallizer. Figure 3.1b illustrates the cross-section of the crystallizer with 2.7 centimeters diameter and 10 centimeters height. Thermal couple number one (T1) was located at the top of the bed, T2 at the middle of the bed, T3 at the bottom of the bed, and the horizontal T4 at the bottom of the bed.

3.2.2 Hydrate Formation Procedure

Each sample (amino acids and surfactants) was dissolved in the deionized water. This solution was placed into the crystallizer and immersed in a cooling water bath. To make sure the system was clean, methane was used to purge the crystallizer three times, followed by injecting methane into the reservoir and keeping gas free in the crystallizer. After the water bath chilled the reservoir's temperature down to a preferable value, at 2 °C, the reservoir gas was released suddenly into the crystallizer to reach hydrate formation pressure. Finally, hydrate formation data was recorded every 10 seconds into the computer. Every experiment was carried out in the quiescent condition with a fixed water and gas in the system. While the hydrate formed, the pressure was decreased due to methane gas consumption to form a crystal and the temperature raised by exothermic reaction effects. A formation experiment was continued until the recorded pressure was not significantly changed. The gas uptake (gas consumption) was calculated by the change of thermodynamic data (pressure and temperature), following Equation 3.1 (Babu *et al.*, 2013).

$$\Delta n_{H,\downarrow} = n_{H,0} - n_{H,t} = \left(\frac{PV}{zRT} \right)_{G,0} - \left(\frac{PV}{zRT} \right)_{G,t} \quad (3.1)$$

Where $\Delta n_{H,\uparrow}$ = moles of consumed gas for hydrate formation (mole)

$n_{H,t}$ = moles of hydrate at time t, (mole)

$n_{H,0}$ = moles of hydrate at time 0, (mole)

P = pressure of the crystallizer, (atm)

T = temperature of the crystallizer, (K)

V = the volume of the gas phase in the crystallizer, (cm³)

Z = compressibility factor

R = the universal gas constant 82.06 cm³•atm/mol•K

Subscripts of G, 0 and G, t represents the gas phase at time zero and time t respectively. The conversion of water to hydrate is calculated in Equation 3.2 (Babu *et al.*, 2013).

$$\text{Conversion of water (\%)} = \frac{\Delta n_{H,\downarrow} \times \text{hydration number}}{\Delta n_{H_2O}} \times 100 \quad (3.2)$$

3.2.3 Hydrate Dissociation Procedure

Thermal stimulation technique was selected to perform the dissociation process after the hydrate formation finished approximately around for fourteen hours. The pressure of the free gas in the system was reduced by venting out to the desired pressure. Water bath started heating the crystallizer up to approximately 30 °C and was marked that starting point as time zero, which accumulated the total mole of gas in the system ($n_{H,0}$). At any time given, the number of moles remained ($n_{H,t}$), so that the number of moles of gas released from hydrate at any time during dissociation was calculated by Equation 3.3 (Siangsai *et al.*, 2015).

$$\Delta n_{H,\uparrow} = n_{H,0} - n_{H,t} = \left(\frac{PV}{zRT} \right)_{G,0} - \left(\frac{PV}{zRT} \right)_{G,t} \quad (3.3)$$

Where $\Delta n_{H,\uparrow}$ = moles of consumed gas for hydrate formation (mole)

$n_{H,t}$ = moles of hydrate at time t, (mole)

$n_{H,0}$ = moles of hydrate at time 0, (mole)

P = pressure of the crystallizer, (atm)

T = temperature of the crystallizer, (K)

V = the volume of the gas phase in the crystallizer, (cm³)

Z = compressibility factor

R = the universal gas constant 82.06 cm³•atm/mol•K

Subscripts of G, 0 and G, t represent the gas phase at time zero and time t respectively. The percentages of methane recovery were calculated by Equation 3.4, as a function of time for any dissociation experiment based on its information of formation experiment (Siangsai *et al.*, 2015).

$$\% \text{ methane recovery} = \frac{(\Delta n_{H,\uparrow})}{(\Delta n_{H,\downarrow})} \times 100 \quad (3.4)$$

CHAPTER IV

RESULTS AND DISCUSSION

In this work, two amino acids and two surfactants were selected to study their effects on the methane hydrate formation and dissociation. The concentrations of surfactants, namely sodium dodecyl sulfate (SDS) and methyl ester sulfonated (MES) were varied, 0.06 wt%, 0.12 wt% (CMC-MES), and 0.23 wt% (CMC-SDS), and 0.03 wt%, 0.06 wt%, 0.012 wt% and 0.23 wt% respectively. For amino acids, l-leucine was varied the concentration at 0.12 wt%, 0.23 wt%, 0.5 wt%, and 0.7 wt% and l-valine was at 0.12 wt%, 0.23 wt%, 0.5 wt%, 0.7 wt%, and 0.9 wt%. This study was carried out in a quiescent condition at 8 MPa and 2 °C. After gas hydrates were completed, thermal stimulation method was used to dissociate the hydrates by increasing the temperature to 30 °C.

4.1 Effects of L-leucine

4.1.1 Methane Hydrate Formation

Table 4.1 shows methane hydrate formation experimental conditions with the presence of l-leucine at different concentrations. The investigation is focused mainly on the gas uptake, which means the amount of methane gas converted to hydrates. From the results, using 0.5 wt% l-leucine solution results in higher gas consumed to hydrates than 0.23 wt% and 0.7 wt% l-leucine. A possible reason that increasing l-leucine concentration to 0.7 wt% slightly decreases the methane consumption is due to the mechanism of amino acid inhibition effects. There is the possibility of hydrophobic-hydrophobic interactions between the non-polar side chains prevents agglomeration and forms a rigid hydrate film at the liquid/gas interface, having the hydrate cages half empty (Bhattacharjee *et al.*, 2016). In addition, a lower concentration of l-leucine could attribute to the extremely porous nature of hydrates that help to overcome the mass transfer resistance at a greater extent than at a higher concentration (Veluswamy *et al.*, 2017). However, solutions with the lower concentrations (0.12 wt% and 0.23 wt%) do not enhance hydrate formation because the surface activity with these concentrations is not low enough (Liu *et al.*, 2015).

Table 4.1 Methane hydrate formation experimental conditions with the presence of l-leucine at 8 MPa and 2 °C

Exp. #	Concentration [wt%]	Induction Time [mns]	Total CH ₄ Uptake [mol of gas/mol of H ₂ O]	Conversion [%]
1	0.12	N/A	N/A	N/A
2	0.23	76.33	0.026	15.15
3	0.5	7.16	0.167	96.24
4	0.5	17.83	0.173	99.48
5	0.5	32.83	0.171	98.17
Average			0.170 ± 0.003	97.96 ± 1.63
6	0.7	254.67	0.163	93.81
7	0.7	211.67	0.158	90.75
8	0.7	260.33	0.165	94.99
Average			0.162 ± 0.004	93.18 ± 2.19

As the hydrate formation is an exothermic process, it can be noticed by the temperature spikes in the temperature profile during the formation (Veluswamy *et al.*, 2016). Four thermocouples were placed in different positions inside the crystallizer, T1 at the top, T2 at the middle, T3 at the bottom, and T4 horizontally at the bed of the reactor. In general, the process of methane hydrate formation starts from gas dissolution into the liquid phase. Afterward, the solution reaches a supersaturated condition to accommodate a hydrate growth (Khurana *et al.*, 2017). Gas uptake and temperature profile during the methane hydrate formation with l-leucine are shown in Figures 4.1 - 4.3. The mechanism of hydrate formation was promoted by l-leucine occurs in two stages of hydrate nucleation. First hydrate formation probably forms as snowflakes or an open porous hydrate structure that is suspended at the gas/liquid interfaces. Meanwhile, hydrate particles tend to move to the wall of crystallizer and grow upward along the wall (Kalogerakis *et al.*, 1993). Yoslim *et al.* (2010) also claimed that the capillary suction of the liquid from the bulk upward to the free wall can renew the gas-liquid interface of the hydrate growth front. So, it is believed that the hydrate particles are creeping along the wall of crystallizer until it blocks the gas inlet hole, located at the side of crystallizer (Figure 3.1 b), showing the first plateau in the figures. A moment after, hydrates that block the gas inlet hole is cracked, and the

free gas is consumed to form continuously until it reaches the equilibrium, as shown by the second plateau.

The observation of gas uptake and temperature profile of 0.23 wt% l-leucine system shows only slight gas consumption even the temperature starts to spike after 70 minutes, approximately 0.026 mol of gas/ mol of water. It might be claimed that the hydrates formed in a single stage at the interfaces of gas/ liquid with high resistant hydrate film, where there is no more gas diffusion into the water phase for further hydrate formation, as shown in Figure 4.1. Veluswamy *et al.* (2016) also observed that using 0.2 wt% l-leucine solution had no characteristic promotion effect on the hydrate formation.

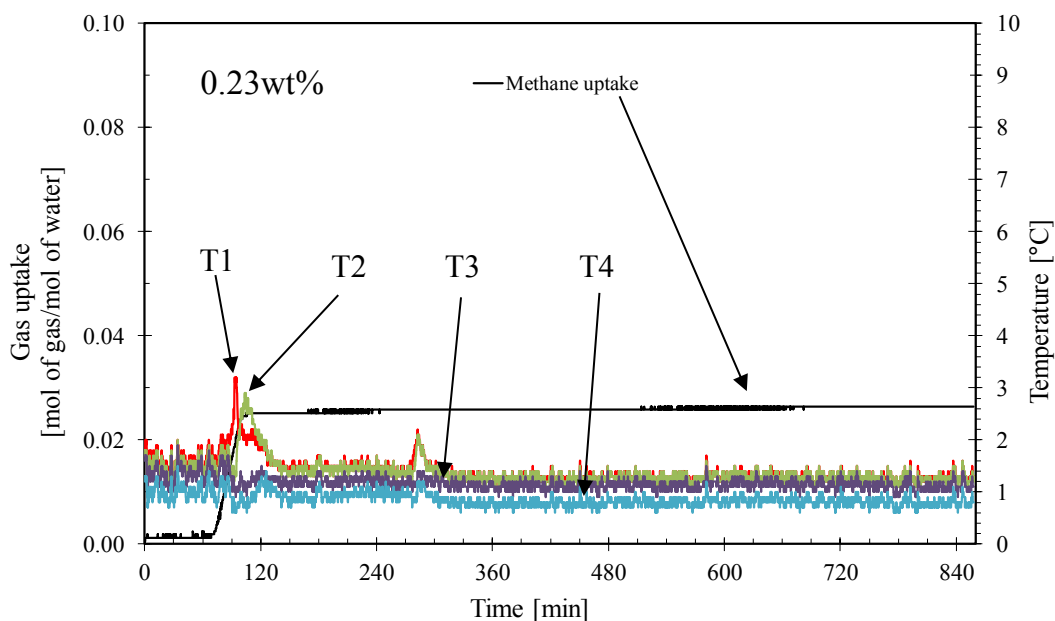


Figure 4.1 Methane uptake and temperature profiles during hydrate formation in the presence of 0.23 wt% at 8 MPa and 2 °C (Experiment 1, Table 2.1).

In contrast, when 0.5 wt% l-leucine is used in the methane hydrate formation, the dissolved gas in the water phase takes about 10 minutes to reach the supersaturated condition before the first nucleation, then the gas consumption is constant till 150 minutes with small gas uptake (0.038 mol of gas/ mol of water), Figure 4.2. After that period, the temperature increases again corresponding to the second nucleation and a sudden big change of gas uptake (0.173 mol of gas/ mol of

water). For 0.7 wt% l-leucine, it takes a longer time to reach the supersaturated condition, approximately over 200 minutes before the hydrates start to grow. However, the gas is consumed steadily at the first nucleation compared to the secondary one, where temperature rises again around 510 minutes, and the gas consumption goes up sharply to reach the maximum value (0.158 mol of gas/ mol of water), Figure 4.3.

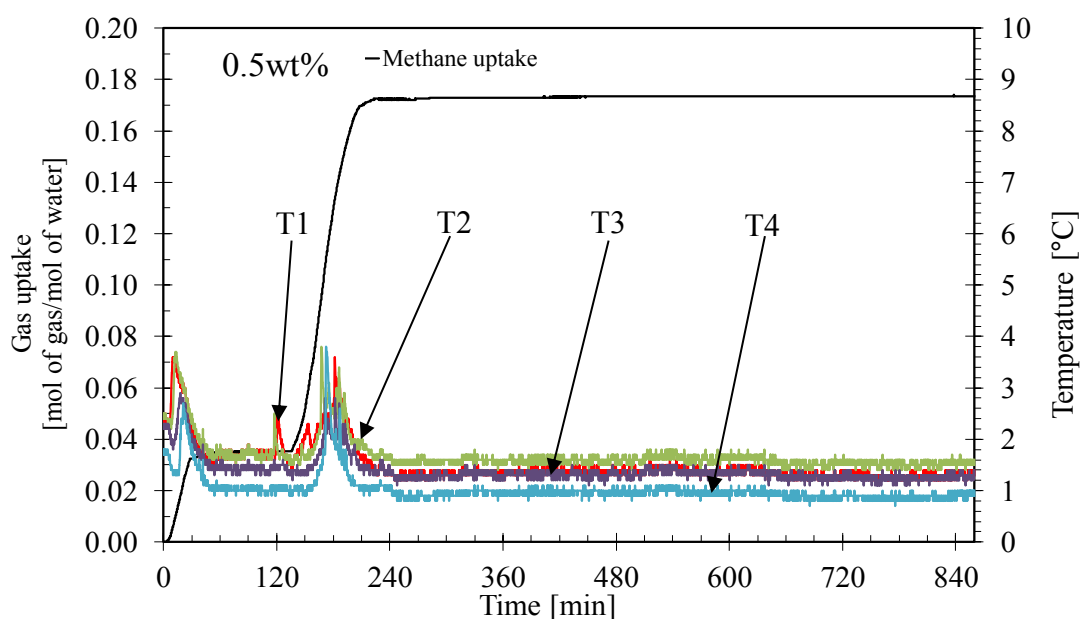


Figure 4.2 Methane uptake and temperature profiles during hydrate formation in the presence of 0.5 wt% at 8 MPa and 2 °C (Experiment 4, Table 4.1).

Figure 4.4 illustrates the methane uptake profiles for the hydrate formation with different concentrations of l-leucine solution at 8 MPa and 2 °C. The hydrate formation shows that the optimum l-leucine concentration of 0.5 wt% results in the highest gas uptake, 0.170 ± 0.003 mol of gas/ mol of water with an average of water conversion to hydrates 97.96 ± 1.63 %. The l-leucine concentration of 0.7 wt% offers lower gas uptake, 0.162 ± 0.004 mol of gas/ mol of water and 93.18 ± 2.19 % water conversion. However, the lower concentration of l-leucine 0.23 wt% seems less influence to promote the hydrate formation. There was no methane hydrate formation with 0.12 wt% l-leucine.

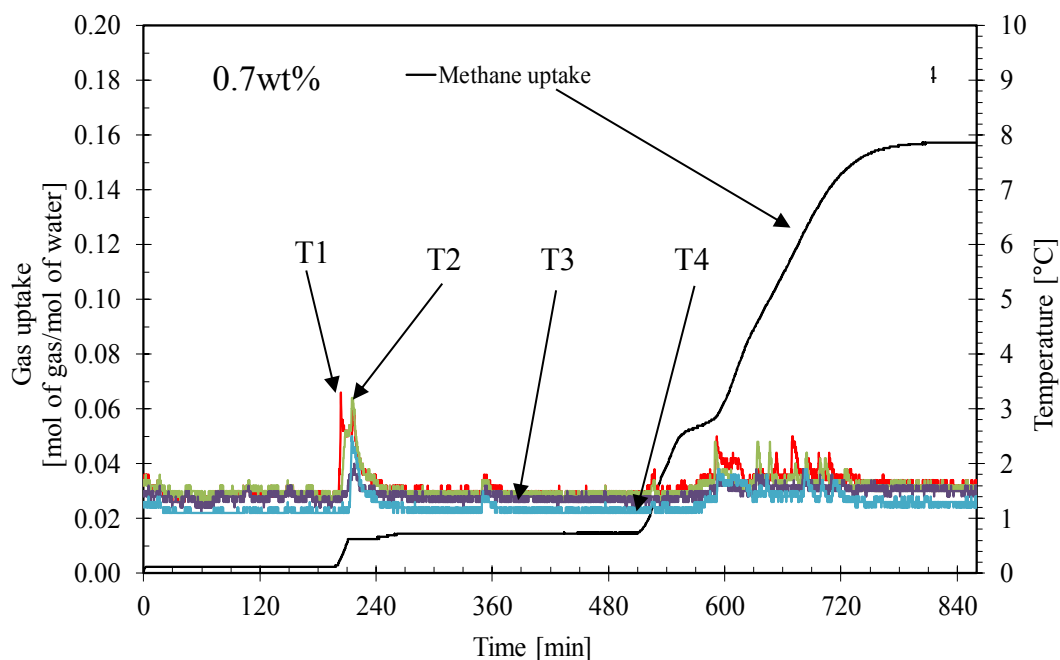


Figure 4.3 Methane uptake and temperature profiles during hydrate formation in the presence of 0.7 wt% at 8 MPa and 2 °C (Experiment 7, Table 4.1).

4.1.2 Methane Hydrate Dissociation

After methane hydrate formation, the gas recovery is conducted to decompose the gas from a solid structure by thermal stimulation technique from 2 to 30 °C. When methane starts to release, there are noticeable changes of temperature profiles of the four thermocouples in the crystallizer due to the heat transfer between the hot water circulation and hydrate dissociation, which is an endothermic process. As seen in Figure 4.5, it can be observed gas start to release at 3.11 °C and the change of temperature profiles of the thermocouples. The decomposed methane release continuously until it reaches the constant. However, the temperature profiles of the four thermocouples illustrate differently in the crystallizer because of different hydrate dissociation regions.

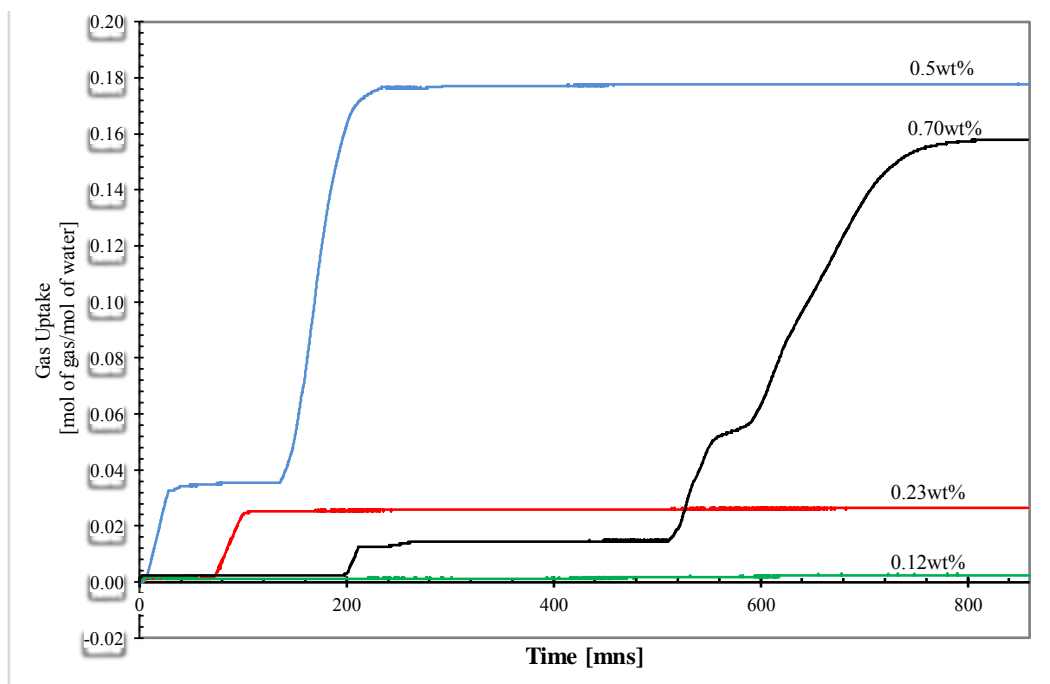


Figure 4.4 Hydrate formation kinetic plots using different l-leucine concentrations (0.7 wt%, 0.5 wt%, and 0.23 wt% and 0.12 wt%) in an unstirred reactor at 8 MPa and 2 °C (Experimental # 2, 5, and 7, Table 4.1).

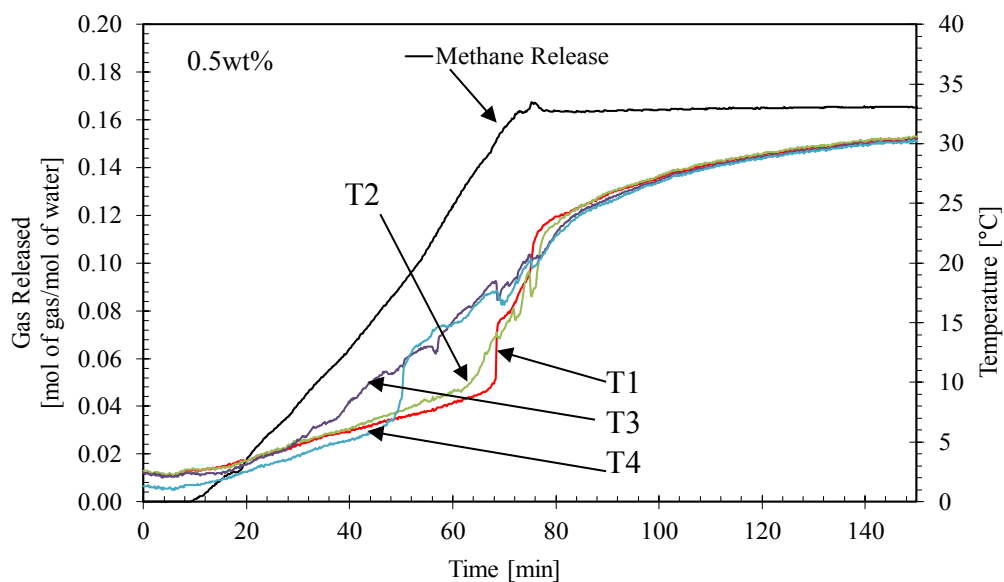


Figure 4.5 Methane released and temperature profiles for the decomposition of hydrates formed with 0.5 wt% l-leucine with temperature driving force of 28 °C (Experiment 12, Table 4.2).

Table 4.2 Methane hydrate dissociation at 30 °C from the hydrates formed with different l-leucine concentrations from the formation temperature 2 °C

Exp. #	Concentration [wt%]	ΔT^a [°C]	Dissociation Temperature T_d^b [°C]	CH ₄ Released [mol /mol of H ₂ O]	CH ₄ Recovery [%]
9	0.12	28	N/A	N/A	N/A
10	0.23	28	N/A	N/A	N/A
11	0.5	28	2.80	0.159	95.10
12	0.5	28	2.50	0.166	95.64
13	0.5	28	3.11	0.162	97.92
Average				0.162 ± 0.004	96.22 ± 1.50
14	0.7	28	3.16	0.158	97.06
15	0.7	28	3.21	0.151	96.12
16	0.7	28	3.05	0.155	94.31
Average				0.155 ± 0.004	95.83 ± 1.39

^a $\Delta T = T_{\text{end}} - T_{\text{start}}$

^b T_d = Dissociation temperature at final formation pressure around 4 MPa

After the temperature inside the crystallizer crosses the equilibrium point, the temperatures of all thermocouples (T1, T2, T3, and T4) increase simultaneously to the maximum dissociation temperature, 30 °C. That observation could be claimed that the hydrate dissociation takes place in all regions once the temperature reaches the dissociation temperature (T_d), but each region takes different times to complete the dissociation.

Table 4.2 shows that methane recovery from the hydrate formation with 0.5 wt% and 0.7 wt% l-leucine is about the same, 96.22 ± 1.50 and 95.83 ± 1.39% respectively. Moreover, Figures 4.5 - 4.6 show hydrate dissociation profiles that demonstrate the gas released and temperature profiles of l-leucine solution with two different concentrations. The dissociation of the hydrates formed with 0.23 wt% and 0.7 wt% starts releasing gas at around 3 °C and reaches plateau around 80 minutes.

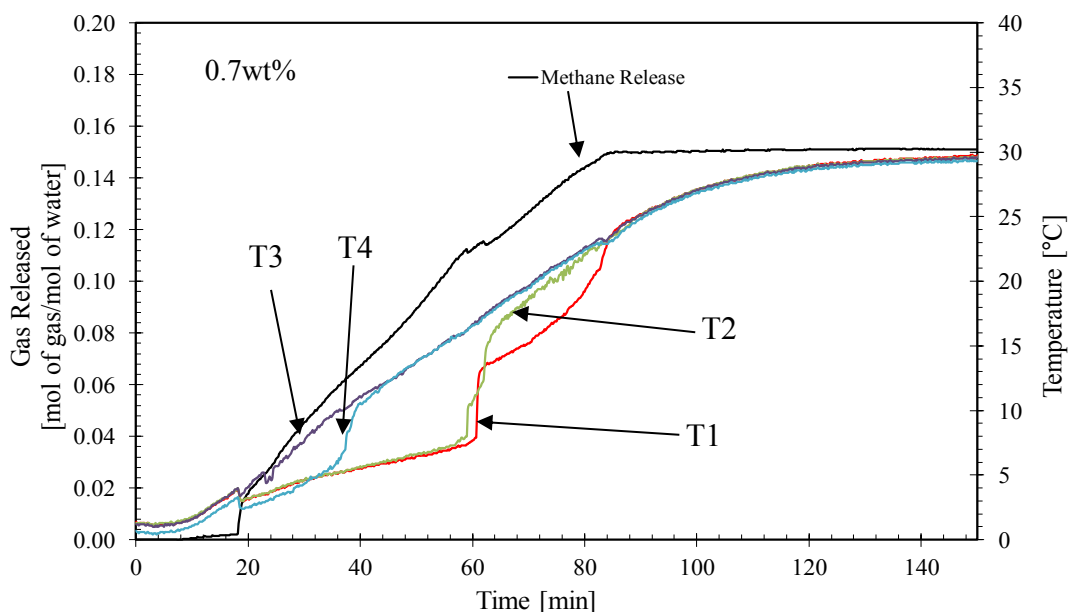


Figure 4.6 Methane released and temperature profiles for the decomposition of hydrates formed with 0.7 wt% l-leucine at temperature driving force of 28 °C (Experiment 15, Table 4.2).

4.2 Effects of L-valine

4.2.1 Methane Hydrate Formation

The experimental results of promoting effects of l-valine are demonstrated in Table 4.3. From the table, l-valine enhances methane hydrate formation when the concentration is at least 0.5 wt%. With 0.5 wt% l-valine, an average methane uptake about 0.137 ± 0.008 mol of gas/ mol of water, equivalent to $78.9 \pm 5.03\%$ water conversion can be obtained. With 0.7 wt% l-valine, the highest gas uptake (approximately 0.171 ± 0.004 mol of gas/ mol of water, $98.21 \pm 2.53\%$ water conversion) can be achieved. However, increasing l-valine to 0.9 wt% results in the adverse effects. The role of l-valine might be from its nature (non-polar aliphatic sidechain, hydrophobic) to affect methane hydrate formation (Veluswamy *et al.*, 2017). Some amino acids (l-valine, l-leucine, l-tryptophan, etc.) were reported to lower surface activity or surface adsorption at gas/liquid interfaces where the first hydrates commonly grow in the system. Typical hydrate nucleation begins from the liquid/gas interface close to the reactor wall, where the temperature is the lowest due to

immersing the stainless-steel reactor into a coolant water circulation bath, as in Figure 3.1a. Finally, methane hydrates grow as a porous structure on the reactor wall, and liquid migrates from the bulk phase to the porous structure due to capillary forces (Liu *et al.*, 2015). Veluswamy *et al.* (2017) also inferred distinctly the hydrate promotion effect, with nonpolar hydrophobic amino acids (tryptophan and leucine) promoting methane hydrate formation at least 5–10 times faster than that of polar basic hydrophilic amino acids (histidine and arginine), which include l-valine under this work. Cai *et al.* (2017) also mentioned that the behavior of the amino acid in promoting or inhibiting hydrate formation slightly depended on the nature of the amino acid (polarity, aliphatic or aromatic side-chains and length of side-chains) and its interaction with the guest molecule during hydrate formation.

Table 4.3 Methane hydrate formation experimental conditions with the presence of l-valine at 8 MPa and 2 °C

Exp. #	Concentration [wt%]	Induction Time [mns]	Total CH ₄ Uptake [mol of gas/mol of H ₂ O]	Conversion [%]
19	0.12	N/A	N/A	N/A
20	0.23	N/A	N/A	N/A
21	0.5	9.67	0.147	84.74
22	0.5	5.33	0.132	75.86
23	0.5	2.24	0.132	76.18
		Average	0.137 ± 0.008	78.92 ± 5.03
24	0.7	92.33	0.173	99.81
25	0.7	92.67	0.173	99.54
26	0.7	68.15	0.166	95.29
		Average	0.171 ± 0.004	98.21 ± 2.53
27	0.9	26.17	0.157	90.56
28	0.9	19.53	0.158	91.32

There has been also reported that the inhibiting nature of amino acids on methane and natural gas hydrate formation was observed at concentrations ≥ 0.5 mol % (corresponding to 2.05, 2.45, 2.9, and 3.2 wt% for glycine, alanine, serine, and proline respectively), which are greater than the maximum concentration of 0.9 wt% employed in this work. It can be inferred that apart from the nature of amino acids, the

concentration employed also plays a key role in affecting the methane hydrate formation kinetics (Sa *et al.*, 2016).

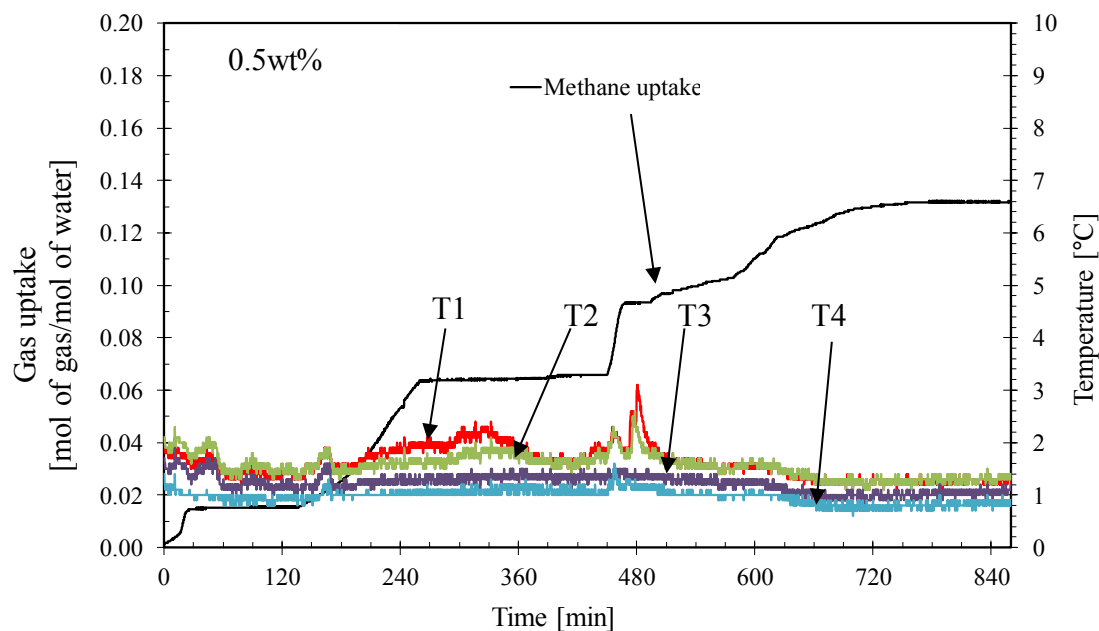


Figure 4.7 Methane consumption and temperature profiles during hydrate formation in the presence of 0.5 wt% l-valine at 8 MPa and 2 °C (Experiment 21, Table 4.3).

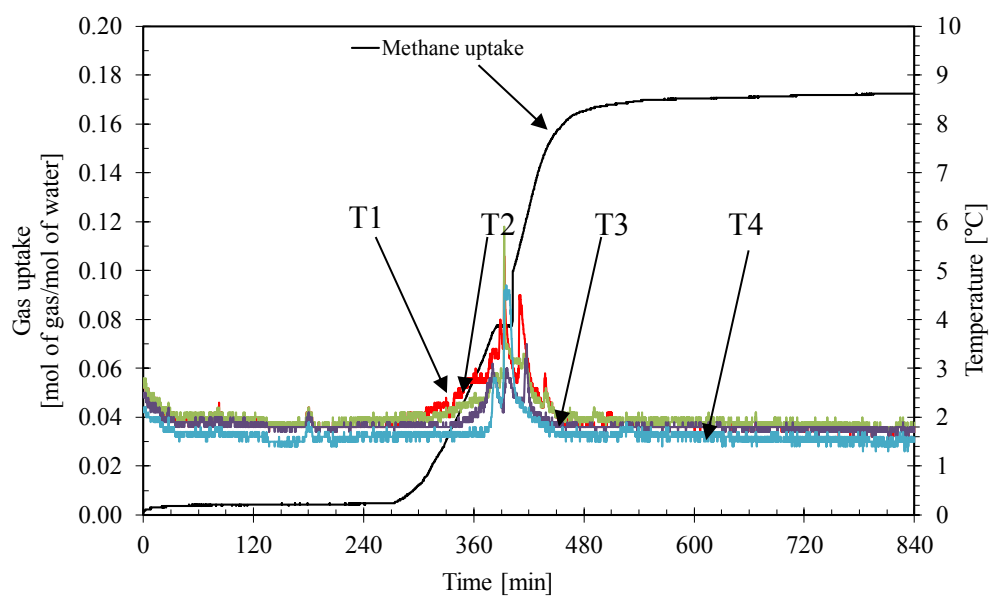


Figure 4.8 Methane consumption and temperature profiles during hydrate formation in the presence of 0.7 wt% l-valine at 8 MPa and 2 °C (Experiment 25, Table 4.3).

Figure 4.7 shows the gas uptake and temperature profiles of methane hydrate formation with 0.5 wt% l-valine. It takes a very long time (about 750 minutes) to achieve the complete formation with few stages of gas consumption behavior. Moreover, Figure 4.8 presents the gas uptake and temperature profiles of hydrate formation with 0.7 wt% l-valine. The induction time of this system is around 270 minutes and the formation completes at 540 minutes.

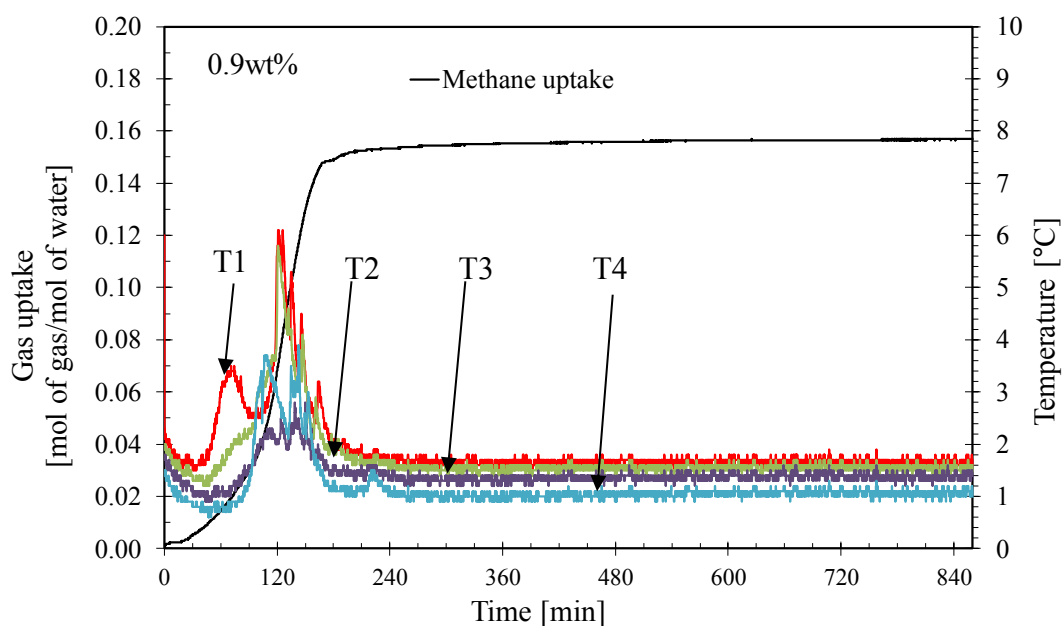


Figure 4.9 Methane uptake and temperature profiles during hydrate formation in the presence of 0.9 wt% l-valine at 8 MPa and 2 °C (Experiment 27, Table 4.3).

However, Figure 4.9 exhibits clearly that 0.9 wt% l-valine could achieve faster methane hydrate formation rate, reaching the constant gas uptake in approximately 300 minutes. Faster methane hydrate formation rate, approximately 300 minutes to reach the constant as shown in Figure 4.9, can be observed with 0.9 wt% l-valine at a lower gas uptake (maximum 0.158 mol of gas/ mol of water, 91.32 % water conversion) than using 0.5 wt% and 0.7 wt% at the same experimental condition. A reason might be the mechanism of a typical amino acid. A higher concentration offers a faster kinetic and slightly decreases the methane uptake. That behavior was first reported by Veluswamy *et al.* (2017) when methane hydrates formed with l-tryptophan. The effects could be claimed that methane uptake using 0.9 wt% l-valine

offers faster initial kinetics; the initial hydrates thus formed offer increased mass transfer resistance for methane in the gas phase to access the unconverted solution to enable further hydrate formation (gas uptake) (Veluswamy *et al.*, 2017).

4.2.2 Methane Hydrate Dissociation

Table 4.4 shows methane hydrate dissociation from the systems with l-valine at different experimental concentrations. The results present that the decomposition temperature of every concentration starts slightly below 3 °C, while the total methane release depends on the methane consumption from the formation. However, the encaged methane gas in the hydrates might not totally be released, because there is some gas still remaining in the water (Linga *et al.*, 2009).

Table 4.4 Methane hydrate dissociation at 30 °C from the hydrates formed with different l-valine concentrations from the formation temperature 2 °C

Exp. #	Concentration [wt%]	ΔT [°C]	Dissociation Temperature T_d [°C]	CH ₄ Released [mol /mol of H ₂ O]	CH ₄ Recovery [%]
29	0.23	28	N/A	N/A	N/A
30	0.5	28	3.61	0.141	95.52
31	0.5	28	2.52	0.127	96.52
32	0.5	28	2.53	0.128	94.12
				Average 0.147 ± 0.008	96.72 ± 1.31
33	0.7	28	2.80	0.166	96.08
34	0.7	28	2.23	0.164	94.44
35	0.7	28	3.10	0.156	94.06
				Average 0.162 ± 0.010	94.86 ± 1.07
36	0.9	28	2.71	0.151	96.09
37	0.9	28	2.45	0.153	96.92

The dissociation for hydrates formed with different concentrations is shown in Figure 4.10. The methane gas released and temperature profiles follow the dissociation pattern of l-leucine systems. The gas released reaches the plateau approximately below 100 minutes with the same temperature driving force at 28 °C. It is clearly seen that methane gas releases faster with higher methane uptake (0.7 wt%

l-valine system). Veluswamy *et al.* (2017) reported the dissociation kinetics of amino acid system that when concentration of amino acid was increased, there was a slight improvement in the rate of gas release.

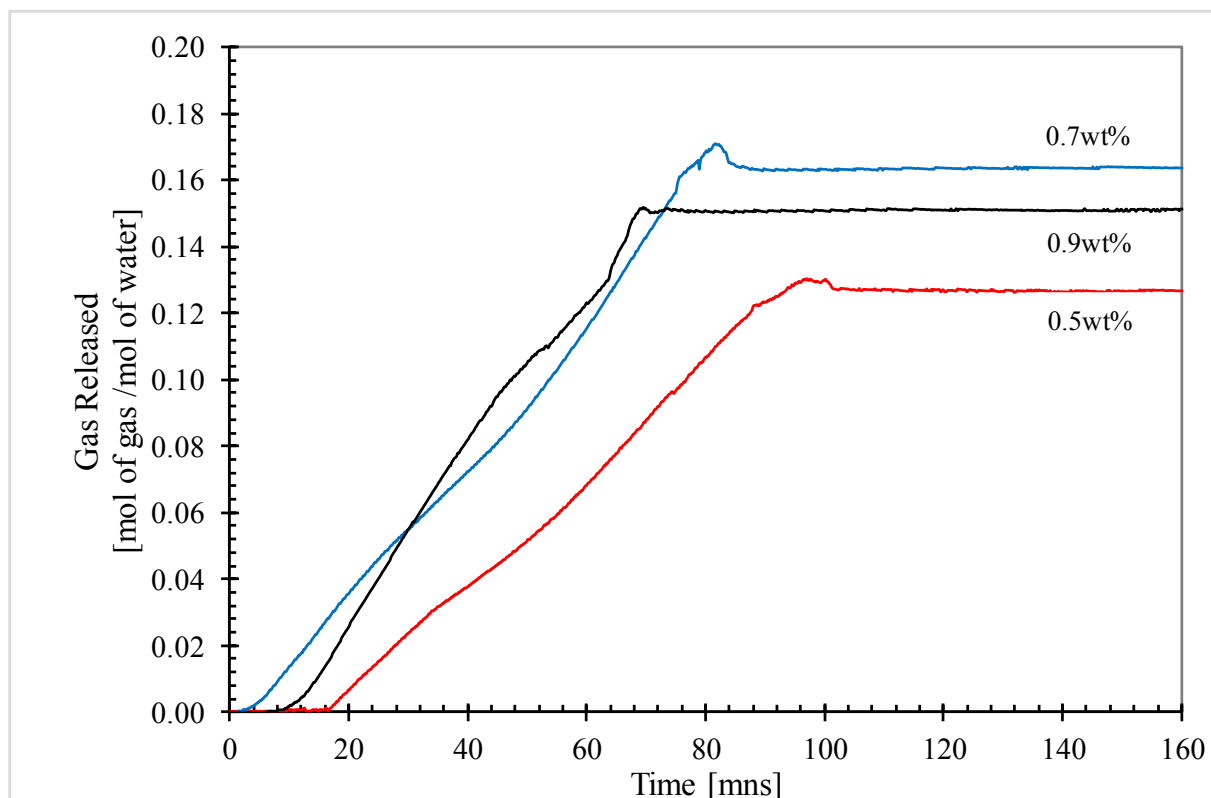


Figure 4.10 Hydrate dissociation kinetic plots using different l-valine concentrations (0.9 wt%, 0.7 wt%, and 0.5) in an unstirred reactor at 30 °C (Experimental # 29, 32 and 34, Table 4.4).

4.3 Effects of Sodium Dodecyl Sulfate (SDS)

4.3.1 Methane Hydrate Formation

Sodium dodecyl sulfate (SDS, an anionic surfactant) has a long history in roles of the kinetic promoter for hydrate formation. Kalogerakis *et al.* (1993) reported that SDS significantly altered the surface or interfacial free energy; therefore, SDS has the direct effects on hydrate formation due to surfactant form a colloidal-size cluster, namely micelles in the experimental solution. At a specific concentration of

surfactant (CMC), micelle changes surprisingly almost every physical property that depends on the size or number of particles in solution.

On the other hand, SDS influences hydrate nuclei formation in the bulk water, the agglomerating particles move rapidly to be adsorbed on the solid surface at the water-gas interface. Radial growth proceeds and forms concentric layers of hydrates, which are held by the walls until the cell is filled with hydrates. Meanwhile, the level of free water in the bottom of the crystallizer decreases when particles are removed from the water and attached to the stainless-steel walls as in this study. The adsorption of hydrate surfactant particles on the metal surface prevents the hydrate particles from hindering further reactions in the free water, allowing the initial high rate of hydrate formation (Zhong and Rogers, 2000). As such, methane hydrate formation in Table 4.5 shows great kinetics and capacity uptake in the quiescent solution. However, at the highest SDS concentration, 0.23 wt%, offers slightly lower gas consumption than the concentration of 0.12 wt%, because the presence of SDS causes the water not to be converted into hydrates completely. In other words, higher initial SDS concentration, the lower final percent conversion of water into hydrates and then smaller apparent storage capacity (Lin *et al.*, 2004)

Figure 4.11 illustrates gas consumption respect to time of different SDS concentrations, 0.23 wt% (CMC), 0.12 wt% and 0.06 wt%. The two higher concentrations, CMC, and 0.12 wt%, provide similar great gas uptake and higher than the system with 0.06 wt%. These high capacities were explained well by Ganji *et al.* (2007). Using surfactant (SDS), the solubility of the hydrocarbon gas in water increases and finer hydrate particle formation occurs in water. This causes a higher surface area and therefore a higher mass transfer rate. On the other hand, surfactants are anti-agglomerates that prevent hydrate crystals to agglomerate causing less free water to entrap between solid hydrates.

However, significant alterations in hydrate formation rates is noted well below this CMC value, 0.23 wt%, as shown in Table 4.6, specifically as low as 0.12 wt% and 0.06 wt% SDS. Since pressure, temperature, and the presence of hydrocarbon gas could affect CMC, whose behavior to initiate hydrate formation mechanism. Results were found that the hydrate induction time decreases with decreasing the concentrations. This shorter induction time in the surfactant solution is possibly

because of spatial uniformity of micellar nuclei sites containing precise amounts of guest gas, which contrast to randomness of induction time with no surfactant (Zhong and Rogers, 2000).

The changes to lower CMC of SDS to enhance hydrate formation kinetics and methane uptake was also reported by Ganji *et al.* (2007). They claimed that CMC of a surfactant solution depends on temperature, pressure and the nature of the hydrate-forming gas and may be well below the CMC measured by the standard method at atmospheric pressure and room temperature.

Table 4.5 Methane hydrate formation experimental conditions with the presence of SDS at 8 MPa and 2 °C

Exp #	Concentration [wt%]	Induction Time [mins]	Total CH ₄ Uptake [mol of gas/mol of H ₂ O]	Conversion [%]
38	0.06	14.57	0.101	56.02
39	0.06	36.50	0.104	58.89
40	0.12	20.50	0.164	94.34
41	0.12	16.17	0.165	95.21
42	0.23	43.00	0.163	93.86
43	0.23	30.17	0.165	95.15

The observation of gas uptake from Figure 4.11 shows that SDS concentration of 0.06 wt% takes about 20 minutes to reach the plateau, while 0.23 wt% takes around 50 minutes to complete the formation. This behavior was proven by Kalogerakis *et al.* (1993), who expressed that the kinetics increased with the increase in the pressure and the decrease in concentration the of SDS. So, the behavior of two stages hydrate formation was not occurred clearly in this work.

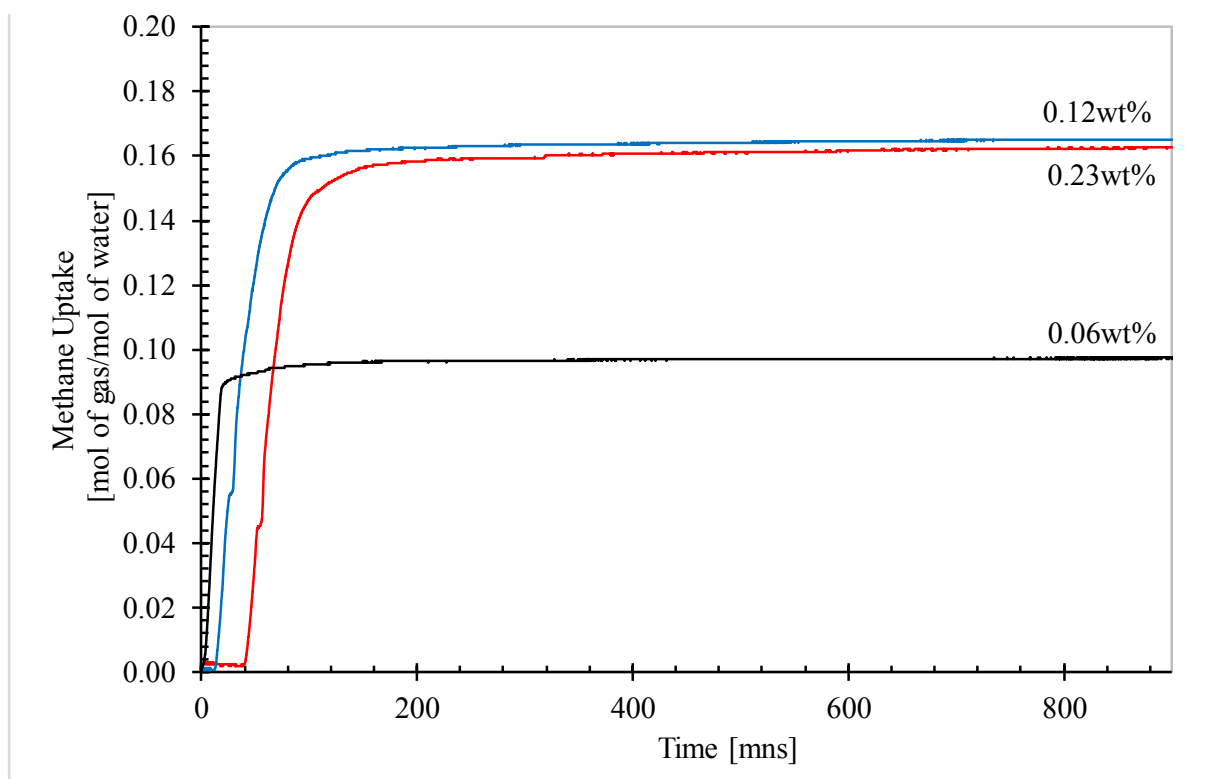


Figure 4.11 Hydrate formation kinetic plots using different SDS concentrations (0.23 wt%, 0.12 wt%, and 0.06 wt%), in an unstirred reactor at 2 °C and 8 MPa (Experimental # 38, 41 and 42 Table 4.5).

4.3.2 Methane Hydrate Dissociation

After the hydrates were formed by promoters as described above, they are dissociated to recover the methane gas from the solid hydrates. As the result in Table 4.6, methane gas releases from two higher concentration, 0.23 wt% and 0.12 wt%, systems at about the same dissociation temperature, 2.40 °C and methane released, 0.155 mol of gas/mol of water. So, the effects of different concentrations of SDS on methane dissociation is not noticeable if those concentrations enhance the gas uptake about the same extent.

Table 4.6 Methane hydrate dissociation conditions with different SDS concentrations at temperature 30 °C

Exp. #	Concentration [wt%]	ΔT [°C]	Dissociation Temperature T_d [°C]	CH ₄ Released [mol /mol of H ₂ O]	CH ₄ Recovery [%]
44	0.06	28	3.95	0.095	97.66
45	0.06	28	4.15	0.101	99.10
46	0.12	28	2.42	0.155	93.89
47	0.12	28	2.36	0.157	95.16
48	0.23	28	2.36	0.155	94.94
49	0.23	28	2.32	0.158	95.77

Figure 4.12 shows the methane release diagram of SDS system at different concentrations. The graphs are noticed clearly that with two higher methane gas consumption concentrations, they release gas higher rates with the same shape to reach the plateau which takes about 110 minutes. At lower concentration (0.06 wt%), the delay in the dissociation kinetics, noticeably higher dissociation temperature (4 °C), and about the same period to complete gas recovery can be observed.

4.4 Effects of Methyl Ester Sulfonate (MES)

4.4.1 Methane Hydrate Formation

Sodium methyl ester sulfonate (MES) is grouped in a synthesized anionic surfactant, which is possible to reduce significant surface tension in its aqueous solution and reported the positive effects on methane hydrates recently (Chaturvedi *et al.*, 2018). Table 4.7 presents the results of promoting effects of MES at different concentrations and at the same experimental condition as the other three promoters above. The methane uptake of four higher concentrations, 0.06 wt%, 0.12 wt%, 0.23 wt%, and 0.5 wt%, provides greatly about the same yield of hydrate formation (over 90 % water conversion to hydrates), while the lowest concentration of 0.03 wt% offers a little gas uptake. The greatly enhanced methane hydrate formation in the presence of these higher anionic surfactant concentrations is mainly because of increased solubility of gas molecules in the aqueous phase and entrainment the gas at the interface,

ordering the water molecules to reach the entrapment within the different unit cells of hydrate structure (Chaturvedi *et al.*, 2018). Ganji *et al.* (2007) also reported micelle formation and formation of foam increase solubility of methane gas in water in the presence of surfactant above CMC.

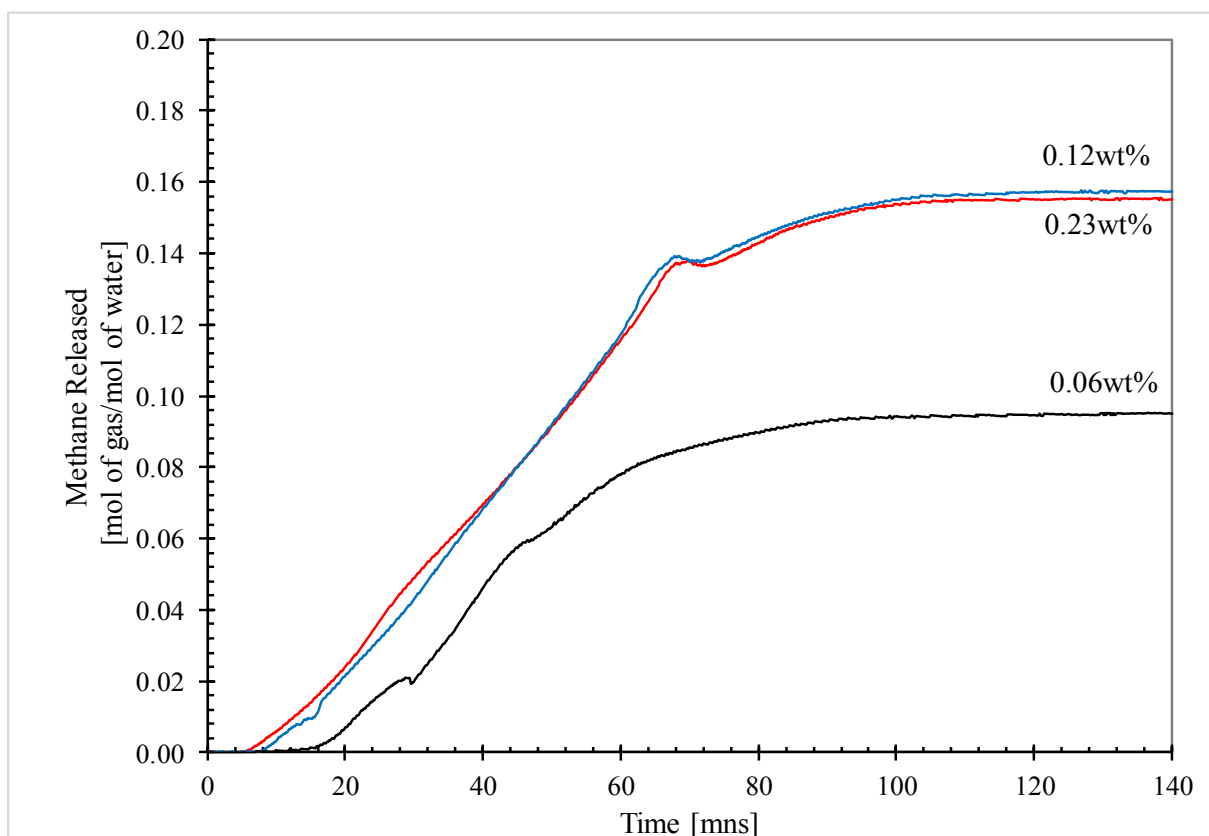


Figure 4.12 Hydrate dissociation kinetic plots using different SDS concentrations (0.23 wt%, 0.12 wt%, and 0.06 wt%) in an unstirred reactor at dissociation temperature 30 °C (Experimental # 44, 47 and 48, Table 4.6).

However, the lower concentration, 0.03 wt%, exhibits two stages of hydrate formation with the lowest conversion. That phenomenon might be claimed that MES at 0.03 wt% hardly lowers the interfacial tension that leads to methane hydrate formation at interfaces, which limit the mass transfer to bulk water. Then, the hydrates grow further along the reactor wall and in the gas phase, causing probably blockage inlet gas. After that blockage hydrate particle cracked, methane is consumed as seen in the second stage, and grow further above the liquid phase.

Table 4.7 Methane hydrate formation experimental conditions with the presence of MES at 2 °C and 8 MPa

Exp. #	Concentration [wt%]	Induction Time [mns]	Total CH ₄ Uptake [mol of gas/mol of H ₂ O]	Conversion [%]
50	0.03	12.16	0.071	42.73
51	0.03	11.35	0.067	38.67
52	0.06	14.52	0.163	93.90
53	0.06	12.83	0.153	88.42
54	0.12	276.00	0.162	93.11
55	0.12	142.30	0.165	95.09
56	0.12	10.20	0.170	98.12
Average			0.16 ± 0.005	95.44 ± 2.52
57	0.23	250.50	0.153	88.14
58	0.23	338.50	0.160	92.03
59	0.23	4.47	0.163	94.43
Average			0.159 ± 0.005	91.53 ± 3.17
60	0.5	5.50	0.173	99.87
61	0.5	6.67	0.169	96.96
62	0.5	3.17	0.173	99.33
Average			0.172 ± 0.002	98.72 ± 1.54

Figure 4.13 presents the hydrate formation profiles with the time taken of different concentrations. The effects of MES on methane hydrate formation is noticeable with the hydrate formation rate reaches the constant gas consumption around 100 minutes and takes less than 20 minutes of induction time of every concentration. The fast kinetics are because of the typical property of MES influence to the mechanism of hydrate formation. In other words, its solutions have lower surface tension and formation of micelles to increase the solubility of a gas in the liquid phase. These behaviors accelerate the mass transfer from the bulk to the hydrate phase (Zhang *et al.*, 2008).

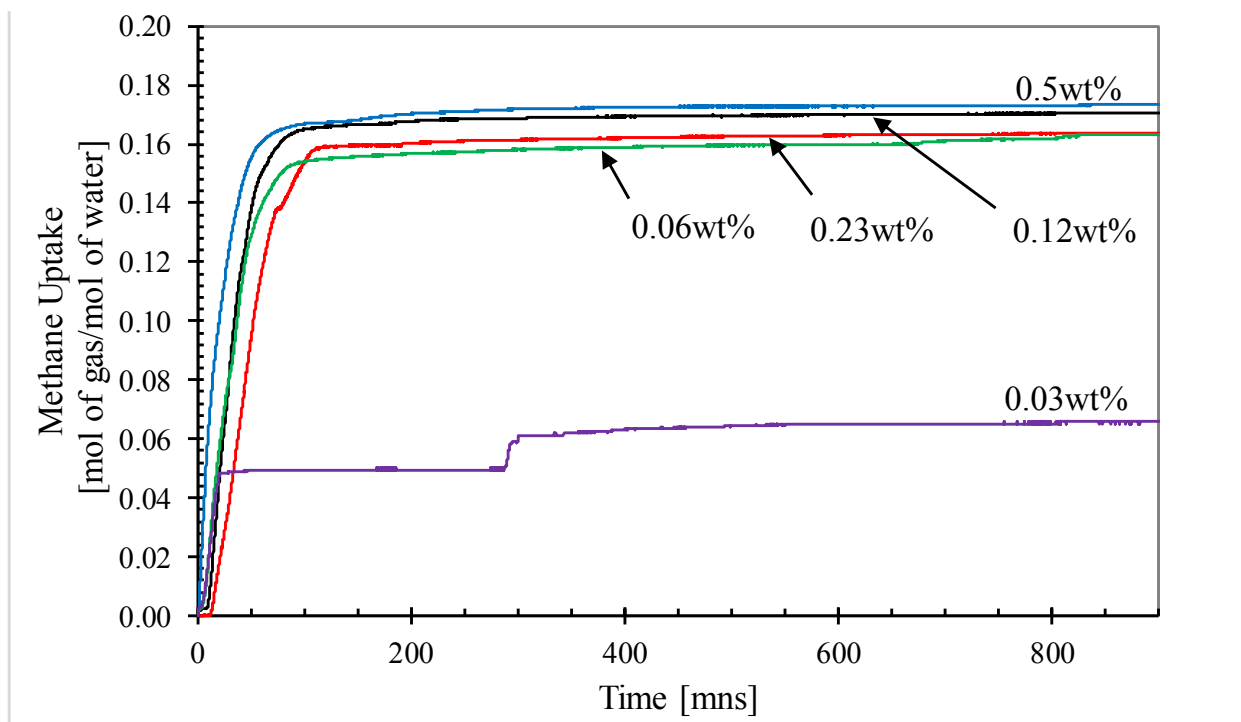


Figure 4.13 Hydrate formation kinetic plots using different MES concentrations (0.5 wt%, 0.23 wt%, 0.12 wt%, 0.06 wt%, and 0.03 wt%), in an unstirred reactor at 2 °C and 8 MPa (Experimental # 51, 52, 56, 59 and 62, Table 4.7).

4.4.2 Methane Hydrate Dissociation

Dissociation of MES system is exhibited in Table 4.8, which indicates that methane gas recovery could achieve approximately more 90 percent in every concentration. From the table, methane hydrates with MES at different concentrations start to release gas at around 2.5 °C.

Graphical plots of methane dissociation with MES is presented in Figure 4.14 and illustrates the effects of different concentrations. It is clearly seen that higher concentrations, 0.5 wt%, 0.23 wt%, 0.12 wt%, 0.06 wt%, offer a very similar pattern of methane dissociation profile. Gas released plateaus start to release around 10 minutes and reach the stable level about 100 minutes, while the lower concentration, 0.03 wt%, releases gas over 20 minutes and completes gas recovery at a shorter period, about 60 minutes.

Table 4.8 Methane hydrate dissociation conditions with different MES concentration at 30 °C

Exp. #	Concentration [wt%]	ΔT (°C)	Dissociation Temperature, T_d [°C]	CH ₄ Released [mol /mol of H ₂ O]	CH ₄ Recovery [%]
63	0.03	28	2.58	0.068	92.06
64	0.03	28	2.47	0.064	96.59
65	0.06	28	2.54	0.156	95.56
66	0.06	28	2.73	0.149	95.89
67	0.12	28	2.34	0.158	98.08
68	0.12	28	2.45	0.159	96.49
69	0.12	28	2.53	0.162	95.39
Average				0.160 ± 0.002	96.65 ± 1.35
70	0.23	28	2.36	0.146	95.59
71	0.23	28	2.53	0.154	97.92
72	0.23	28	2.54	0.159	97.18
Average				0.153 ± 0.007	96.89 ± 1.19
73	0.5	28	2.38	0.163	93.51
74	0.5	28	2.16	0.161	95.27
75	0.5	28	2.83	0.159	93.25
Average				0.161 ± 0.002	94.01 ± 1.10

4.5 Comparison

4.5.1 Hydrate Formation at a Concentration of 0.23 wt%

The four promoters (l-leucine, l-valine, SDS and MES) were conducted the experiences at the same conditions of temperature and pressure, 2 °C and 8 MPa in a quiescent solution. Figure 4.15 presents the hydrate formation of each promoter at the same concentration of 0.23 wt%. It is clearly seen that SDS and MES enhance the hydrate formation rate and gas uptake better than l-leucine and l-valine at this specific concentration. This higher kinetic and methane uptake are the results of the surfactant property, which decreases the interfacial free energy, as shown in Table 4.9.

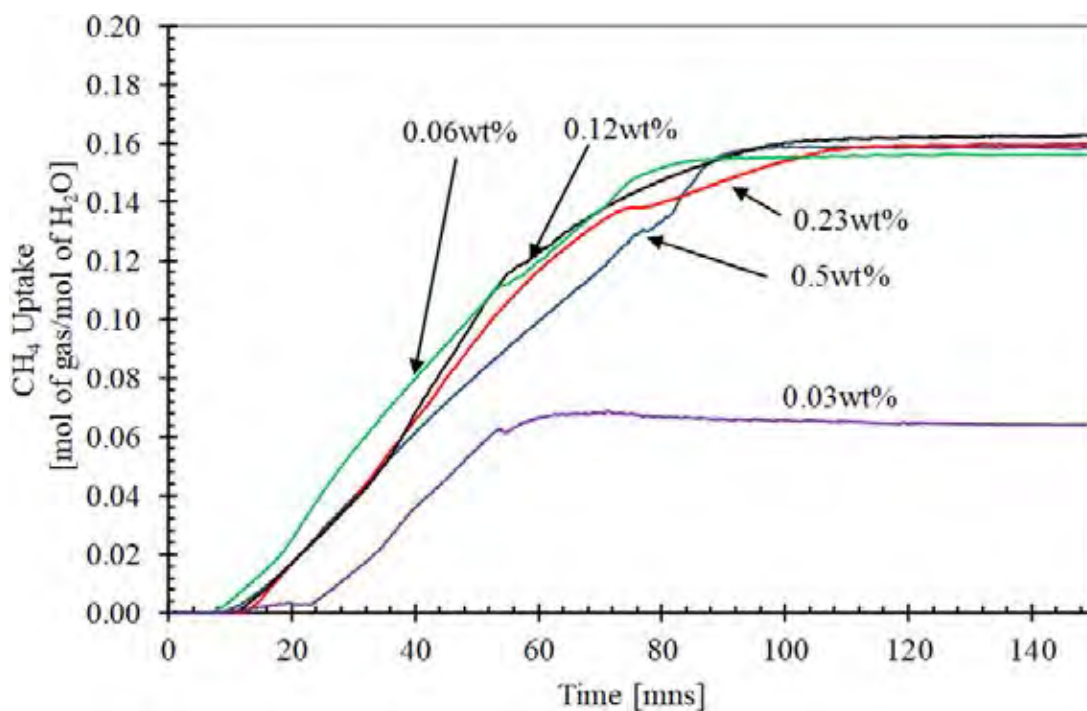


Figure 4.14 Hydrate dissociation kinetic plots using different SDS concentrations (0.03 wt%, 0.06 wt%, 0.12 wt%, 0.23 wt% and 0.5 wt%) in an unstirred reactor at dissociation temperature 30 °C (Experimental # 64, 66, 69, 72 and 75, Table 4.8).

Table 4.9 Surface tension versus concentrations of l-leucine, l-valine, SDS and MES (Liu *et al.*, 2015; Kile and Chiou, 1989; Chaturvedi *et al.*, 2018)

Concentration [wt%]	Surface tension mN/m			
	Leucine	Valine	SDS	MES
0.23	72.5	73.5	42	37
0.50	71.0	73.0	44	37
0.70	69.0	72.0	46	37

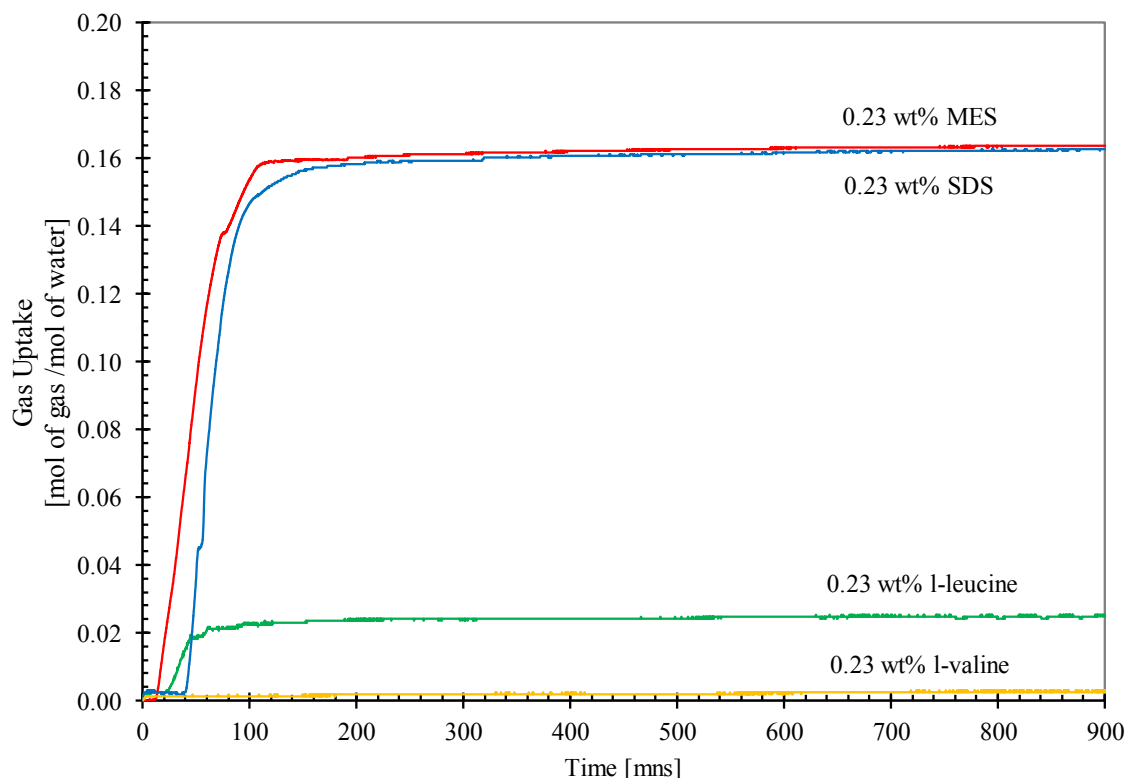


Figure 4.15 Hydrate formation kinetic plots using concentration 0.23 wt% (CMC-SDS) of different promoter (l-leucine, l-valine, SDS and SDS) in an unstirred reactor at 2 °C and 8 MPa (Experimental # 7, 55, 41 and 27).

4.5.2 Hydrate Formation at CMC and Optimum Concentration of Amino Acids

Above description reports the effects of different promoters on methane hydrate formation and dissociation at 2 °C and 8 MPa in quiescent solution. Table 4.10 demonstrates the results of each promoter that enhances the remarkable methane hydrate formation at different concentrations. The results clearly show the effect of l-leucine and l-valine to promote water conversion to hydrates up to approximately 99% or about 0.173 mol of gas/mol of water (Experimental 80 and 82, Table 4.10). However, with SDS and MES, lightly lower conversion, 95% or around 0.163 mol of gas/ mol of water (Experimental 76, 77, 78 and 79, Table 4.10) is obtained. Lui *et al.* (2015) also reported that 0.2 wt% SDS enhanced methane uptake slightly lower than 0.5 wt% l-leucine in the same experimental condition (273 K, 7-9.5 MPa).

Table 4.10 Methane hydrate formation with the presence of CMC-surfactants and optimum concentration of amino acids at 2 °C

System	Exp. #	Formation Temperature [°C]	Concentration [wt%]	Induction Time [mns]	Total CH ₄ Uptake [mol of gas/mol of H ₂ O]	Conversion [%]
SDS	76	2	0.23	43.00	0.163	93.86
	77	2	0.23	30.17	0.165	95.15
MES	78	2	0.12	11.23	0.170	98.12
	79	2	0.12	139.30	0.165	95.09
L-leucine	80	2	0.50	17.83	0.173	99.48
	81	2	0.50	32.83	0.171	98.17
L-valine	82	2	0.70	92.33	0.173	99.81
	83	2	0.70	92.67	0.173	99.54

Figure 4.16 exhibits the hydrate formation profiles at 2 °C and clearly indicates that the surfactants provide fast kinetics to complete hydrate formation, approximately 120 minutes, while l-leucine and l-valine take about 240 minutes and 540 minutes respectively with two stages of formation.

In addition, methane hydrate formation was also conducted at 4 °C and 8 MPa and dissociation at the same temperature driving force, 28 °C. Table 4.11 indicates that the addition of surfactants result in enhancing methane uptake at a higher temperature (4 °C) compared to the amino acids in this study. In other words, SDS and MES achieve the gas uptake up to 0.127 and 0.124 mol of gas/mol of water respectively, but these two surfactants cannot accomplish as high as that formed at 2 °C. Hydrate formation with the presence of surfactants no longer starts to form a thin film at the water-gas interface but starts at the crystallizer wall (gas/metal/liquid) and forms as a think bulky layer. Then, hydrate particles grow upward along the wall and radial growth takes place along the gas/liquid interface, which creates a mushy hydrate layer to cover the interfaces and grows toward the bulk water (Yoslim *et al.*, 2010).

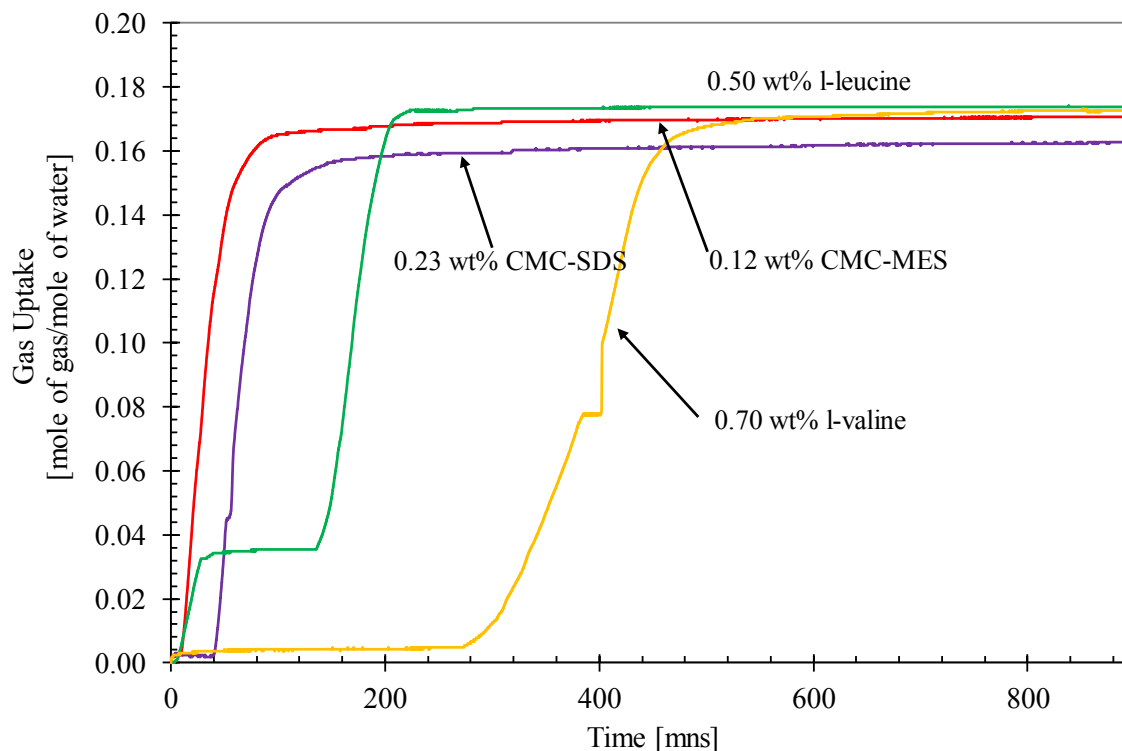


Figure 4.16 Hydrate formation of SDS, MES, l-valine, and l-leucine at CMC-SDS (0.23wt%), CMC-MES (0.12wt%), l-valine (0.7wt%), and l-leucine (0.5wt%) respectively, at 2 °C (Experimental # 76, 78, 80, and 83, Table 4.10).

Table 4.11 Methane hydrate formation with the presence of CMC-surfactants and optimum concentration of amino acids at 4 °C

System	Exp. #	Formation Temperature [°C]	Concentration [wt%]	Induction Time [mns]	Total CH ₄ Uptake [mol of gas/mol of H ₂ O]	Conversion [%]
SDS	84	4	0.23	42.67	0.123	70.51
	85	4	0.23	12.17	0.127	74.89
MES	86	4	0.12	10.33	0.112	65.23
	87	4	0.12	21.33	0.124	71.71
L-leucine	88	4	0.50	29.83	0.075	43.33
	89	4	0.50	26.67	0.078	45.74
L-valine	90	4	0.70	N/A	N/A	N/A

Figure 4.17 shows methane hydrate formation profiles at 4 °C, and it can be noticed that the surfactants also enhance hydrate formation rate and methane uptake more than the amino acids. SDS and MES solutions achieve the plateau level of complete formation around 140 minutes, while l-leucine takes about 380 minutes to reach the plateau, but with l-valine, no hydrate formation at 4 °C is obtained. A broad range of hydrate formation temperature of surfactants might be well explained that solubilization of surfactants drives supersaturated guest molecules, which helps the mass transfer from a bulk phase to hydrates and provides the driving force for the complexation between host molecules (water) and guest molecules in a gas hydrate formation process; furthermore, when the solution of the surfactant concentration exceeds the critical micelle concentration (CMC), the surfactant in an aqueous solution will transform to micelles. Most of the gas molecules are bound to form clusters with water molecules, which promotes the formation of crystal nuclei of gas hydrates (Zhang *et al.*, 2008).

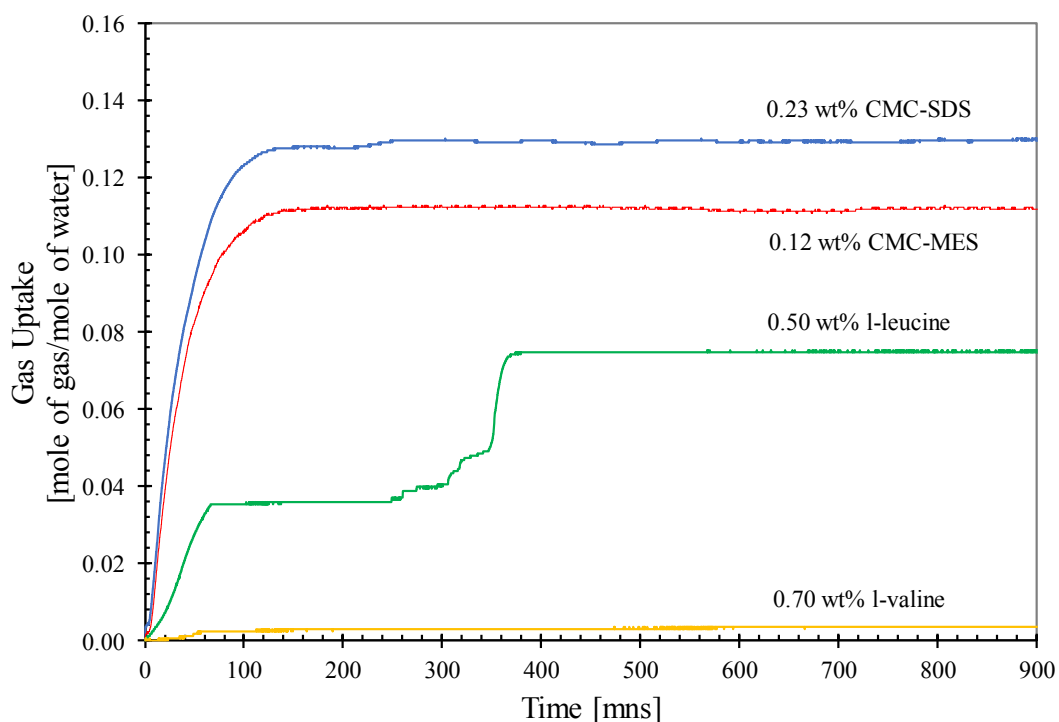


Figure 4.17 Hydrate formation of SDS, MES, l-valine, and l-leucine at CMC-SDS (0.23wt%), CMC-MES (0.12wt%), l-valine (0.7wt%), and l-leucine (0.5wt%) respectively, at 4 °C (Experimental # 85, 86, 88 and 90, Table 4.11).

4.5.3 Methane Hydrate Dissociation at CMC-surfactants and Optimum Concentration of Amino Acids at 2 °C and 4 °C

Table 4.11 shows the experimental data of methane hydrate dissociation at 30 °C. It is clearly seen that every system releases gas below 3 °C with approximately gas recovery higher than 95%. Figure 4.18 presents the hydrate dissociation profiles with time. It shows that the presence of amino acids in the formation speeds up the dissociation to complete around 80 minutes, while with the surfactants, dissociation takes longer, approximately 110 minutes. The dissociation of surfactants' system produces huge amount of foam (Liu *et al.*, 2015; Veluswamy *et al.*, 2018) blocking the gas released in the form of bubbles.

Table 4.12 Methane hydrate dissociation conditions with different promoters at temperature 30 °C from formation temperature at 2 °C

System	Exp. #	Concentration [wt%]	ΔT [°C]	Dissociation Temperature T_d [°C]	CH ₄ Released [mol /mol of H ₂ O]	CH ₄ Recovery [%]
SDS	91	0.23	28	2.36	0.155	94.94
	92	0.23	28	2.32	0.158	95.77
MES	93	0.12	28	2.34	0.158	98.08
	94	0.12	28	2.25	0.159	96.49
L-leucine	95	0.50	28	2.50	0.166	95.64
	96	0.50	28	2.88	0.162	97.92
L-valine	97	0.70	28	2.80	0.166	96.08
	98	0.70	28	2.23	0.164	94.44

Table 4.13 Methane hydrate dissociation conditions with different promoters at temperature 30 °C from formation temperature at 2 °C at 4 °C

System	Exp. #	Concentration [wt%]	ΔT [°C]	Dissociation Temperature T_d [°C]	CH ₄ Released [mol /mol of H ₂ O]	CH ₄ Recovery [%]
SDS	99	0.23	26	5.11	0.117	95.66
	100	0.23	26	4.92	0.122	95.43
MES	101	0.12	26	4.58	0.109	96.21
	102	0.12	26	4.67	0.119	95.79
L-leucine	103	0.50	26	6.42	0.071	92.09
	104	0.50	26	5.76	0.073	91.41
L-valine	105	0.70	26	N/A	N/A	N/A

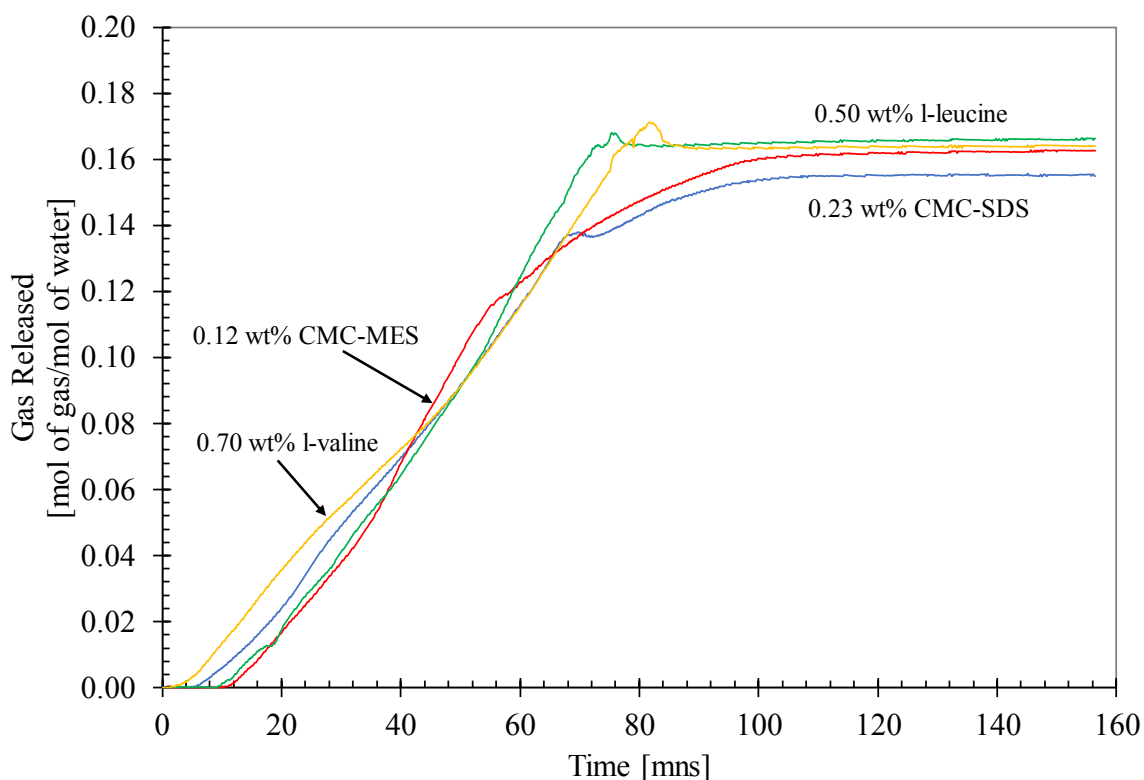


Figure 4.18 Hydrate dissociation of SDS, MES, l-valine, and l-leucine at CMC-SDS (0.23wt%), CMC-MES (0.12wt%), l-valine (0.7wt%), and l-leucine (0.5wt%) respectively, at 30 °C (Experimental # 91, 93, 95 and 98, Table 4.12).

The dissociation data and graphical plots from the formation of 4 °C are exhibited in Table 4.13 and Figure 4.19, respectively. Methane starts to release from the hydrates formed with a surfactant below 5 °C, unlike the l-leucine system that releases the gas at a temperature slightly above 5 °C. Using SDS in the formation releases the highest gas compared to the other promoters. Regarding very low conversion of amino acids in the quiescent solution at 4 °C, l-leucine system releases also low methane gas compared to SDS and MES.

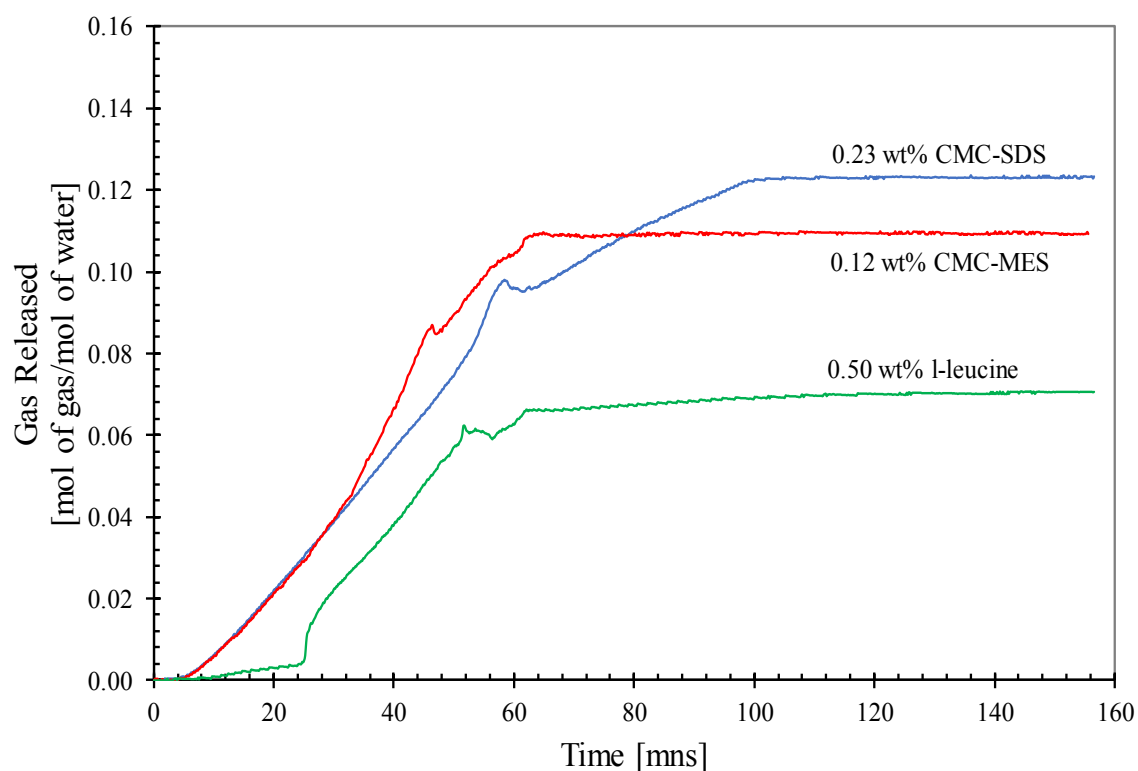


Figure 4.19 Hydrate dissociation of SDS, MES, L-valine, and l-leucine at CMC-SDS (0.23wt%), CMC-MES (0.12wt%), l-valine (0.7wt%), and l-leucine (0.5wt%) respectively, at 30 °C (Experiment # 100, 101 and 103, Table 4.13).

CHAPTER V

CONCLUSION AND RECOMMENDATIONS

5.1 Conclusions

The effects of l-leucine, l-valine, sodium dodecyl sulfate (SDS) and methyl ester sulfonate (MES) on methane hydrate formation at 2 to 4 °C and 8 MPa were investigated in the quiescent solution. L-leucine system formed the hydrates with the maximum methane uptake, approximately 0.170 ± 0.003 mol of gas/mol of water, at 0.5 wt%. Moreover, l-valine at 0.7 wt% was found to give the best enhancement for methane uptake, approximately 0.171 ± 0.004 mol of gas/mol of water. The high gas uptake with SDS was obtained with the concentration above its CMC, 0.23 wt%. MES could influence a high methane uptake with its concentrations around CMC, 0.12 wt%.

At the same concentration, 0.23 wt%, l-leucine and l-valine achieved very low methane uptake and formation rate compared to SDS and MES. The effects of 0.5 wt% l-leucine and 0.7 wt% l-valine on methane hydrate formation and dissociation was compared with using CMC-SDS and CMC-MES at the formation temperature from 2 - 4 °C. Methane hydrate formation with using amino acids at 2 °C provided methane uptake capacity similar to the surfactants, but the formation rate was very slow. However, the hydrates formed at 4 °C with the amino acids resulted in little gas consumption, but the formation with the surfactants still offered the high methane uptake. The dissociated gas from the surfactants produced a lot of foam that could against the gas release, taking a longer time to complete the gas recovery, and losing the amount of surfactants. Unlike the surfactants, methane could be recovered from the hydrates formed with the amino acids at a faster rate and reusability.

5.2 Recommendations

The promoting effects of amino acids on methane hydrate formation have been explained by individual behavior of amino acids, such as hydrate formation morphology with l-leucine and the observation of molecular dynamic (MD) simulation with l-histidine. So, the l-valine solution in this study should be investigated further on its morphology or molecular level to understand its behavior.

The hydrate growth upward to block the inlet gas in crystallizer was observed occasionally and disturbed the promotion capability. Although these promoters can frequently achieve well hydrate formation, the improvement of the gas inlet should be modified ideally.

REFERENCES

- Babu, P., Kumar, R., and Linga, P. (2013). Pre-combustion capture of carbon dioxide in a fixed bed reactor using the clathrate hydrate process. Energy, 50, 364-373.
- Bhattacharjee, G., Choudhary, N., Kumar, A., Chakrabarty, S., and Kumar, R. (2016). Effect of the amino acid l-histidine on methane hydrate growth kinetics. Journal of Natural Gas Science and Engineering, 35, 1453-1462.
- Carroll, J. J. (2004). An examination of the prediction of hydrate formation conditions in sour natural gas. Paper presented at the GPA Europe, Spring Meeting, Dublin.
- Casco, M. E., Martínez-Escandell, M., Gadea-Ramos, E., Kaneko, K., Silvestre-Albero, J., and Rodríguez-Reinoso, F. (2015). High-pressure methane storage in porous materials: are carbon materials in the pole position? Chemistry of Materials, 27(3), 959-964.
- Chatti, I., Delahaye, A., Fournaison, L., and Petitet, J. P. (2005). Benefits and drawbacks of clathrate hydrates: a review of their areas of interest. Energy Conversion and Management, 46(9-10), 1333-1343.
- Chaturvedi, E., Prasad, N., and Mandal, A. (2018). Enhanced formation of methane hydrate using a novel synthesized anionic surfactant for application in storage and transportation of natural gas. Journal of Natural Gas Science and Engineering, 56, 246-257.
- Clennell, M. B., Hovland, M., Booth, J. S., Henry, P., and Winters, W. J. (1999). Formation of natural gas hydrates in marine sediments: 1. Conceptual model of gas hydrate growth conditioned by host sediment properties. Journal of Geophysical Research: Solid Earth, 104(B10), 22985-23003.
- Collett, T. S. (2002). Energy resource potential of natural gas hydrates. AAPG bulletin, 86(11), 1971-1992.
- Demirbas, A. (2010). Methane gas hydrate. Springer London Dordrecht Heidelberg New York: Springer Science & Business Media.
- Englezos, P. (1993). Clathrate hydrates. Industrial & Engineering Chemistry Research, 32(7), 1251-1274.

- Englezos, P., and Lee, J. D. (2005). Gas hydrates: A cleaner source of energy and opportunity for innovative technologies. Korean Journal of Chemical Engineering, 22(5), 671-681.
- Fakharian, H., Ganji, H., Far, A. N., and Kameli, M. (2012). Potato starch as methane hydrate promoter. Fuel, 94, 356-360.
- Ganji, H., Manteghian, M., Omidkhah, M., and Mofrad, H. R. (2007). Effect of different surfactants on methane hydrate formation rate, stability and storage capacity. Fuel, 86(3), 434-441.
- Kalogerakis, N., Jamaluddin, A., Dholabhai, P., and Bishnoi, P. (1993). Effect of surfactants on hydrate formation kinetics. Paper Presented at the SPE International Symposium on Oilfield Chemistry, New Orleans, Louisiana, US.
- Karaaslan, U., and Parlaktuna, M. (2002). Promotion effect of polymers and surfactants on hydrate formation rate. Energy & Fuels, 16(6), 1413-1416.
- Khurana, M., Yin, Z., and Linga, P. (2017). A Review of Clathrate Hydrate Nucleation. ACS Sustainable Chemistry & Engineering, 5(12), 11176-11203.
- Kile, D. E., and Chiou, C. T. (1989). Water solubility enhancements of DDT and trichlorobenzene by some surfactants below and above the critical micelle concentration. Environmental Science & Technology, 23(7), 832-838.
- Koh, C. A. (2002). Towards a fundamental understanding of natural gas hydrates. Chemical Society Reviews, 31(3), 157-167.
- Lin, W., Chen, G.-J., Sun, C.-Y., Guo, X.-Q., Wu, Z.-K., Liang, M.-Y., Yang, L.-Y. (2004). Effect of surfactant on the formation and dissociation kinetic behavior of methane hydrate. Chemical Engineering Science, 59(21), 4449-4455.
- Linga, P., Haligva, C., Nam, S. C., Ripmeester, J. A., and Englezos, P. (2009). Gas hydrate formation in a variable volume bed of silica sand particles. Energy & Fuels, 23(11), 5496-5507.
- Liu, Y., Chen, B., Chen, Y., Zhang, S., Guo, W., Cai, Y., and Wang, W. (2015). Methane Storage in a Hydrated Form as Promoted by Leucines for Possible Application to Natural Gas Transportation and Storage. Energy Technology, 3(8), 815-819.

- Loveday, J. S., and Nelmes, R. J. (2008). High-pressure gas hydrates. Phys Chem Chem Phys, 10(7), 937-950.
- Makogon, Y. F. (2010). Natural gas hydrates – A promising source of energy. Journal of Natural Gas Science and Engineering, 2(1), 49-59.
- Mullin, J. W. (2001). Crystallization. Elsevier , Oxford OX2 8DP 225 Wildwood Avenue, Woburn, MA 01801-2041.
- Nixon, M. F., and Grozic, J. L. (2006). A simple model for submarine slope stability analysis with gas hydrates. Norwegian Journal of Geology/Norsk Geologisk Forening, 86(3), 237-244.
- Sa, J.-H., Kwak, G.-H., Han, K., Ahn, D., Cho, S. J., Lee, J. D., & Lee, and K.-H. (2016). Inhibition of methane and natural gas hydrate formation by altering the structure of water with amino acids. Scientific Reports, 6, 31582.
- Seo, Y.-T., Kang, S.-P., and Lee, H. (2001). Experimental determination and thermodynamic modeling of methane and nitrogen hydrates in the presence of THF, propylene oxide, 1, 4-dioxane and acetone. Fluid Phase Equilibria, 189(1-2), 99-110.
- Servio, P., and Englezos, P. (2003). Morphology study of structure H hydrate formation from water droplets. Crystal Growth & Design, 3(1), 61-66.
- Siangsai, A., Rangsunvigit, P., Kitiyanan, B., Kulprathipanja, S., and Linga, P. (2015). Investigation on the roles of activated carbon particle sizes on methane hydrate formation and dissociation. Chemical Engineering Science, 126 (3), 383-389.
- Sloan, E. J. (2003). Fundamental principles and applications of natural gas hydrates. Nature, 426(6964), 353-363.
- Sloan, E. J. and Koh, C. A. (2007). Clathrate hydrates of natural gases. CRC Press, Colorado School of Mines and Golden, Colorado, U.S.A.
- Veluswamy, Lee, P. Y., Premasinghe, K., and Linga, P. (2017). Effect of Biofriendly Amino Acids on the Kinetics of Methane Hydrate Formation and Dissociation. Industrial & Engineering Chemistry Research, 56(21), 6145-6154.
- Veluswamy, H. P. (2015). Energy storage in clathrate hydrates.

- Veluswamy, H. P., Hong, Q. W., and Linga, P. (2016). Morphology study of methane hydrate formation and dissociation in the presence of amino acid. Crystal Growth & Design, 16(10), 5932-5945.
- Veluswamy, H. P., Kumar, A., Kumar, R., and Linga, P. (2017). An innovative approach to enhance methane hydrate formation kinetics with leucine for energy storage application. Applied Energy, 188(9), 190-199.
- Veluswamy, H. P., Kumar, A., Seo, Y., Lee, J. D., and Linga, P. (2018). A review of solidified natural gas (SNG) technology for gas storage via clathrate hydrates. Applied Energy, 216(11), 262-285.
- Vysniauskas, A., and Bishnoi, P. (1983). A kinetic study of methane hydrate formation. Chemical Engineering Science, 38(7), 1061-1072.
- Yoslim, J., Linga, P., and Englezos, P. (2010). Enhanced growth of methane–propane clathrate hydrate crystals with sodium dodecyl sulfate, sodium tetradecyl sulfate, and sodium hexadecyl sulfate surfactants. Journal of Crystal Growth, 313(1), 68-80.
- Zhang, B.-Y., Qiang, W., and Sun, D.-L. (2008). Effect of surfactant Tween on induction time of gas hydrate formation. Journal of China University of Mining and Technology, 18(1), 18-21.
- Zhong, Y., and Rogers, R. (2000). Surfactant effects on gas hydrate formation. Chemical Engineering Science, 55(19), 4175-4187.

CURRICULUM VITAE

Name: Mr. Kimhak Neak

Date of Birth: November 06, 1992

Nationality: Cambodian

University Education:

2010–2015 Bachelor Degree of Geo-resources and Geotechnical Engineering, Institute of Technology of Cambodia, Phnom Penh, Cambodia

Work Experience:

2015-2017 Position: Business Development

Company name: DKSH (Cambodia) Ltd

2016-Present Position: Chief of Joint Development

Office

Company name: General Department of

Petroleum, Department of International Petroleum Affairs

Poster Presentations:

1. Kimhak, N., Rangsunvigit, P., and Kulprathipanja, S. (2018, October 8-9) Effects of amino acids and surfactants on methane hydrate formation. Paper presented at The 8th International Thai Institute of Chemical Engineering and Applied Chemistry Conference 2018, Pattaya, Thailand.